ARL-TR-9493 ● JULY 2022

DEVCOM ARMY RESEARCH LABORATORY

Design of a Multi-pulse Flash X-ray System for Pulsed X-ray Cineradiography

by Michael B Zellner, Willard C Uhlig, Paul Berning, Brian Wilmer, Nathan Sturgill, Benjamin Huntzinger, and Jennifer Showalter

NOTICES

Disclaimers

The findings in this report are not to be construed as an official Department of the Army position unless so designated by other authorized documents.

Citation of manufacturer's or trade names does not constitute an official endorsement or approval of the use thereof.

Destroy this report when it is no longer needed. Do not return it to the originator.

ARL-TR-9493 ● JULY 2022

Design of a Multi-pulse Flash X-ray System for Pulsed X-ray Cineradiography

Michael B Zellner, Willard C Uhlig, and Paul Berning
DEVCOM Army Research Laboratory

Brian Wilmer
SURVICE Engineering

Nathan Sturgill
IAP Worldwide Services

Benjamin Huntzinger and Jennifer Showalter
Bowhead Cyber Security Solutions & Services, LLC

REPORT DOCUMENTATION PAGE

Form Approved
OMB No. 0704-0188

1. REPORT DATE *(DD-MM-YYYY)*	2. REPORT TYPE	3. DATES COVERED (From - To)
July 2022	Technical Report	1 October 2021–1 May 2022

4. TITLE AND SUBTITLE
Design of a Multi-pulse Flash X-ray System for Pulsed X-ray Cineradiography

5a. CONTRACT NUMBER
W15P7T-17-D-0146/W911QX-20-C-0037

5b. GRANT NUMBER

5c. PROGRAM ELEMENT NUMBER

6. AUTHOR(S)
Michael B Zellner, Willard C Uhlig, Paul Berning, Brian Wilmer, Nathan Sturgill, Benjamin Huntzinger, and Jennifer Showalter

5d. PROJECT NUMBER
AH80

5e. TASK NUMBER

5f. WORK UNIT NUMBER

7. PERFORMING ORGANIZATION NAME(S) AND ADDRESS(ES)
DEVCOM Army Research Laboratory
ATTN: FCDD-RLW-TD
Aberdeen Proving Ground, MD 21005

8. PERFORMING ORGANIZATION REPORT NUMBER
ARL-TR-9493

9. SPONSORING/MONITORING AGENCY NAME(S) AND ADDRESS(ES)

10. SPONSOR/MONITOR'S ACRONYM(S)

11. SPONSOR/MONITOR'S REPORT NUMBER(S)

12. DISTRIBUTION/AVAILABILITY STATEMENT
Approved for public release: distribution unlimited.

13. SUPPLEMENTARY NOTES
ORCID IDs: Michael B Zellner, 0000-0001-7309-312X; Paul Berning, 0000-0001-9699-0245; Willard C Uhlig, 0000-0003-1815-0106

14. ABSTRACT
This work describes the design of a sequencer that combines electrical pulses from multiple Marx generators for use in flash X-radiography systems. The design isolates high-voltage conduction pathways by using field emission effect-based diodes. Combination of two pulses was demonstrated with millisecond temporal separation; however, the method is expandable to an infinite number of pulses. This work also explores influences leading to the millisecond temporal separation. Design modifications are suggested that have the potential to significantly reduce the temporal separation, which are mostly related to controlling the plasma within the diode gap.

15. SUBJECT TERMS
Sciences of Extreme Materials, radiography, flash X-ray, Marx generator, cineradiography, scintillation, capacitor, plasma

16. SECURITY CLASSIFICATION OF:			17. LIMITATION OF ABSTRACT	18. NUMBER OF PAGES	19a. NAME OF RESPONSIBLE PERSON
a. REPORT	b. ABSTRACT	c. THIS PAGE			Michael B Zellner
Unclassified	Unclassified	Unclassified	UU	49	19b. TELEPHONE NUMBER (Include area code) (410) 278-1183

Standard Form 298 (Rev. 8/98)
Prescribed by ANSI Std. Z39.18

Contents

List of Figures

List of Tables

Acknowledgments

Nathan Sturgill is an employee of IAP Worldwide Services and funded under project US Army Combat Capabilities Development Command (DEVCOM) Army Research Laboratory Protection Services, contract number W15P7T-17-D-0146.

Benjamin Huntzinger and Jennifer Showalter are employees of Bowhead Cyber Security Solutions & Services, LLC., Springfield, Virginia. Their research reported in this document was performed in connection with contract W911QX-20-C-0037 with the DEVCOM Army Research Laboratory (ARL). The views and conclusions contained in this document are those of the authors and should not be interpreted as presenting the official policies or position, either expressed or implied, of the DEVCOM ARL or the US Government unless so designated by other authorized documents.

Citation of manufacturer's or trade names does not constitute an official endorsement or approval of the use thereof.

Preface

This work describes design of a multi-pulse flash X-ray system for pulsed X-ray cineradiography. The basic idea of using field emission diodes to combine pulses was conceived in the summer of 2019. A prototype of the system using two 150-kV sources and three 150-kV X-ray tubes (two that acted as blocking diodes and one that acted as a source) was constructed in September 2019. The system was constructed and tested but was only partially successful because we did not account for the impedance and power matching of the sources to the load. Experiments were conducted on October 30, 2019, which showed functionality of the system, but the radiographs indicated very low X-ray flux out of the source. A modified system that used two 300-kV sources to drive the three 150-kV tube system was designed and demonstrated in January 2022. Additional developments such as using magnetic fields to modify the plasma field at the diode junction were conceived and demonstrated in February and March 2022, respectively. Those developments are discussed within this report.

1. Introduction

Multiple scientific disciplines could benefit from development of a many-frame X-radiographic diagnostic that operates with a frame rate near 1 MHz. This capability, however, does not currently exist outside of dedicated multimillion-dollar scientific facilities, as conventional lab-based systems lack the X-ray photon flux and timing to create radiographs of sufficient signal-to-noise ratio. This problem can be addressed through one of three general paths: 1) increase the number of X-ray photons available, 2) increase the sensitivity of the X-ray detection systems, or 3) identify enhanced analysis routines or methods so that a sufficient solution can be reached at currently attainable signal-to-noise ratios.

This work investigates a methodology toward enhancing the number of X-ray photons available by combining off-the-shelf electric capacitive discharge systems (typically referred to as "Flash X-ray Systems") into a single output. Although this method would require an enhanced detector, it would provide a source for multi-frame unified perspective imaging. Figure 1 depicts the basic concept of pulse sequencing. This general framework is infinitely expandable, although practical systems would likely combine only a few independent systems as the cost is linear, and superior technologies, such as laser-driven X-ray generation, would eventually become more cost-effective. This methodology requires two areas of improvement over current systems: 1) creating a device that can combine the electrical pulses while protecting the individual capacitive energy storage systems and 2) designing an X-ray tube output capable of producing X-ray pulses with sufficient output frequency.

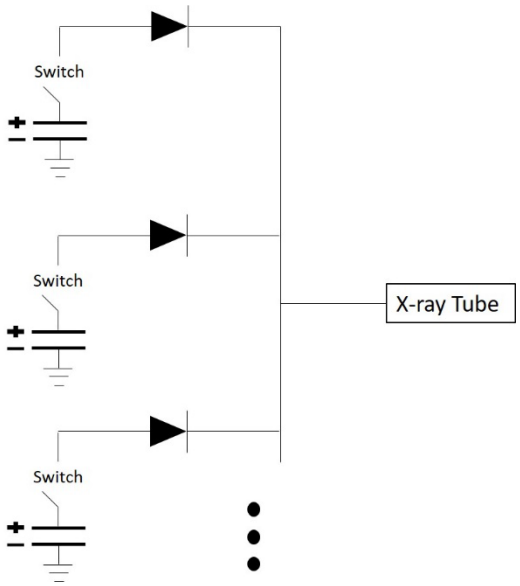

Fig. 1 Schematic depicting the basic concept for pulse sequencing

The method for pulse sequencing proposed here is based upon the utilization of field emission effect[1–3] to isolate current flow. Commercial off-the-shelf field emission effect X-ray vacuum tubes[4,5] are explored for applicability, and improvement modifications are suggested. The suggested improvements relate to the potential of the field emission effect diode to resist reverse current flow with enhanced temporal response. These include investigating the geometry of components related to the field emission process and investigating the generation/dissipation needs of plasma within the diode. Generation of plasma across the diode elements can cause short-circuiting of the diodes, rendering them ineffective. The overall use of field emission effect diodes to isolate high-voltage current flow for X-ray pulse sequencing would incur minimal hardware addition to conventional systems and use as-supplied equipment to charge and discharge the systems.

This work also explores timing aspects of the plasma generation related to relatively simplistic conical-cathode diodes. Here the functionality of the X-ray generating tube was characterized using optical photography to monitor the plasma generation while investigating methods of applying electromagnetic fields local to the field emission diode to influence the plasma. The electrical and radiographic responses were characterized simultaneously to understand any positive or negative influences on the X-ray output.

Finally, this work investigates the applicability of electrical pulse sequencing with regard to potential complications associated with the overall system. This includes investigations of impedance matching components for optimization of power distribution and insulation needs.

2. Results

2.1 Field Emission Effect Diode Method

To combine capacitive flash X-ray systems, field emission effect diodes are investigated to isolate high-voltage current flow. Field emission[1–3] is a quantum mechanical phenomenon in which electrons are extracted from a conductor via application of a strong electric field near the conductor's surface. This phenomenon is theoretically predicted to exist even when the conductor has zero temperature, resulting in the maximum electron energy level equal to the Fermi energy. When sufficient field is applied, the electron emission surface activation barrier is both thinned and reduced in magnitude, therefore increasing the probability of electrons to tunnel through. This phenomenon can be enhanced by slight heating of the

conductor, increasing the number of surface electrons within higher energy states, while remaining below the temperatures that result in thermal emission of electrons.

The field emission effect diodes operate by localized enhancement of the potential field via geometry of the cathode. Figure 2 shows a schematic representation of a typical field emission diode geometry, along with a cartoon depicting equipotential field contours when a potential is applied. This concentration enhances the ability to liberate electrons from the cathode, allowing for conduction to occur across the gap. When a reverse bias is applied (i.e., the field emission enhanced ring becomes the anode and the tungsten rod becomes the cathode in Fig. 2), the lack of field localization points at the cathode reduces the likelihood of electron liberation. Although field concentration occurs near the anode, this potential works to liberate positively charged ions that are bound to the conductor much more strongly than the electronic work function. This combination inhibits current flow.

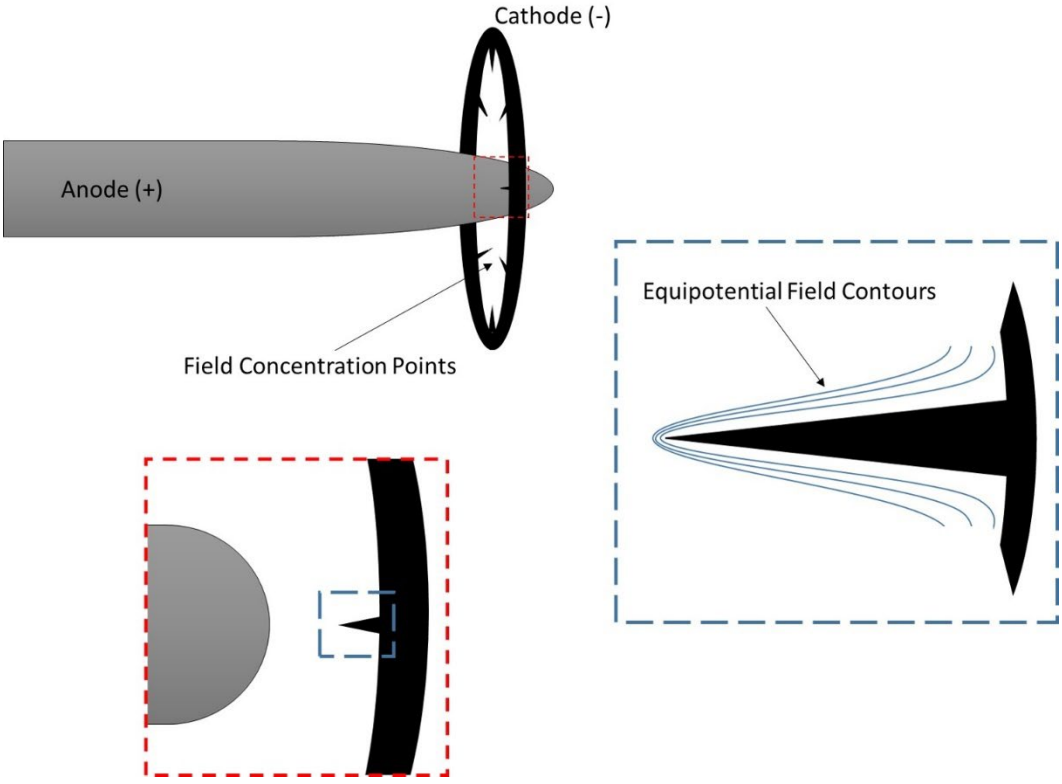

Fig. 2 Schematic representation of a typical field emission diode and a cartoon depicting equipotential field contours near the surface of a pointed structure. The field is concentrated near the tip structure, which enhances the field emission of electrons.

For the purpose of creating a multi-pulse X-ray system, our experiments investigate combining two L3 300 flash X-ray pulsers to drive a 150-kV flash X-ray system source.[4,5] The hardware selection was influenced by what was on-hand, along with the fact that the L3 systems use field emission-based tubes for X-ray generation.

However, if care is taken, a wide range of capacitive-based hardware could be used. Figure 3 shows a schematic of our intended end-state system.

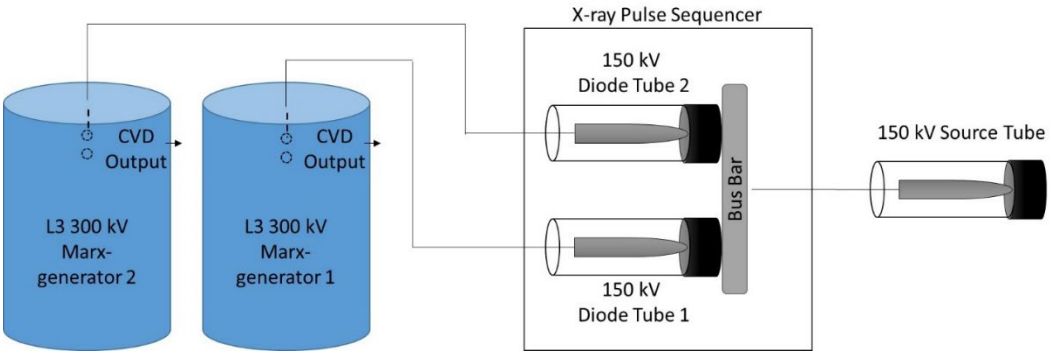

Fig. 3 Schematic depicting a system capable of combining two X-ray flashes into a single head

Functionality of the system relies on the premise that the outgoing pulse interacts with its sequencer diode tube in the conventional geometry, allowing current flow, and in reverse geometry with the sequencer diodes of the other pulse systems, precluding current flow along those paths. An outgoing pulse from Marx generator 1 follows a path to the X-ray source tube by applying a positive potential to the tungsten rod of the X-ray sequencer diode 1, with the ground potential applied to the field emission-enhancing cathode of the source tube. From an electron flow perspective, the X-ray source cathode liberates electrons via the enhanced field emission process to the tungsten rod of the source tube, which is in contact with the bus bar and field emission-enhancing cathode of sequencer diode 1. A second field emission enhanced liberation allows the electrons to flow to the positively charged tungsten rod of the X-ray sequencer diode 1 (anode). This path would not be altered by having a second, charged Marx generation system attached to the line. This is related to the inherent Marx generation configuration and gap protection, which are schematically depicted in Fig. 4.

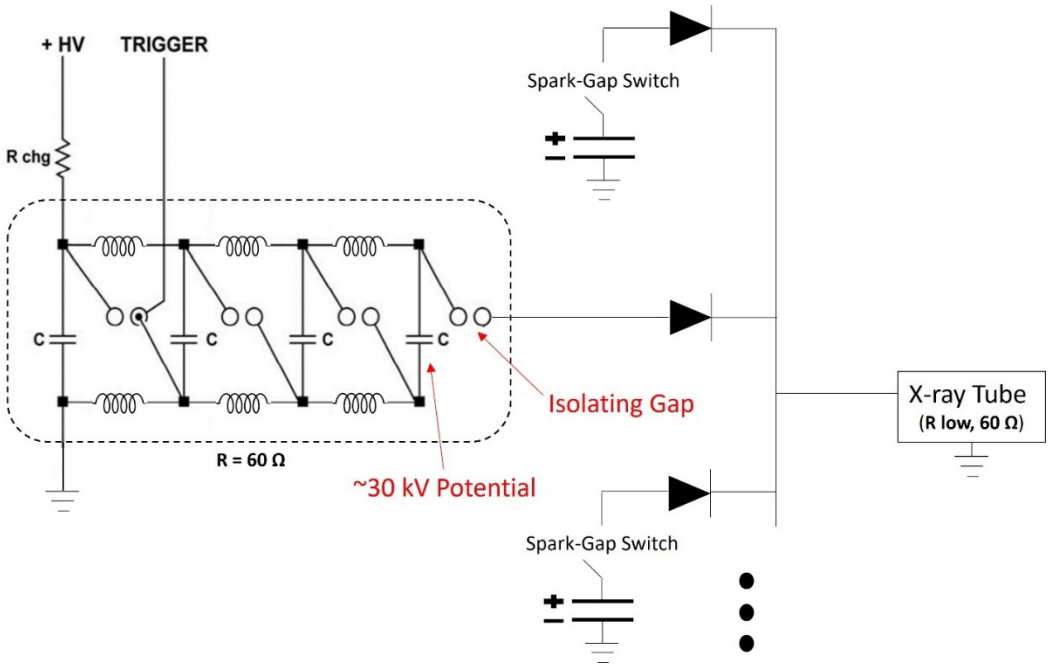

Fig. 4 Notional schematic of a Marx generator depicting the gap protection

From the perspective of the second charged system, diode tube 1 and the X-ray source tube in series act as a voltage divider, resulting in approximately 150-kV standoff potential with diode 2 tube, which is its intended design potential. Without trigger initiation, the end capacitor of the second Marx generator supplies only approximately +30 kV and is gap isolated. This combination is insufficient to establish a current pathway from the first Marx generator to the second or cause the second Marx generator to auto-discharge.

After triggered dissipation of the first Marx generator, and while waiting sufficient time for plasma within the spark gap switches and diode tubes to dissipate, the system becomes ready for triggered discharge of the second Marx generator. Except for the end capacitor, having a +30 kV charge, the possible conduction pathways are similar as previously described but reversed in order. The resistance of current to travel through sequencer diode 2, through sequencer diode 1 to the internals of Marx generator 1 is still precluded, as the path for electron flow in the sequencer diode 1 is opposite its intended direction and includes additional gap isolation. We emphasize here that this mechanism requires the diode tubes to operate in their initial, unaltered state. Deviations, such as plasma generation/accumulation within in the gap, could preclude desired operations. Although this example system would only generate two X-ray pulses, it would be infinitely expandable by adding additional Marx generators and field emission diodes prior to the bus bar.

The X-ray pulse sequencer and cabling for the multi-pulse system were custom made and use air space as the primary means of insulation. At standard temperature and pressure, potentials of 300 kV require approximately 11.5 cm of insulation spacing.[6,7] We designed the box to have a minimum spacing of 15.2 cm and lined the box with 12.7-mm-thick polyethylene and acrylic panels to increase the insulation. The output side of the X-ray sequencer used off-the-shelf L3 150-kV system remote tube heads and cabling. Figure 5 shows the sequencer construction.

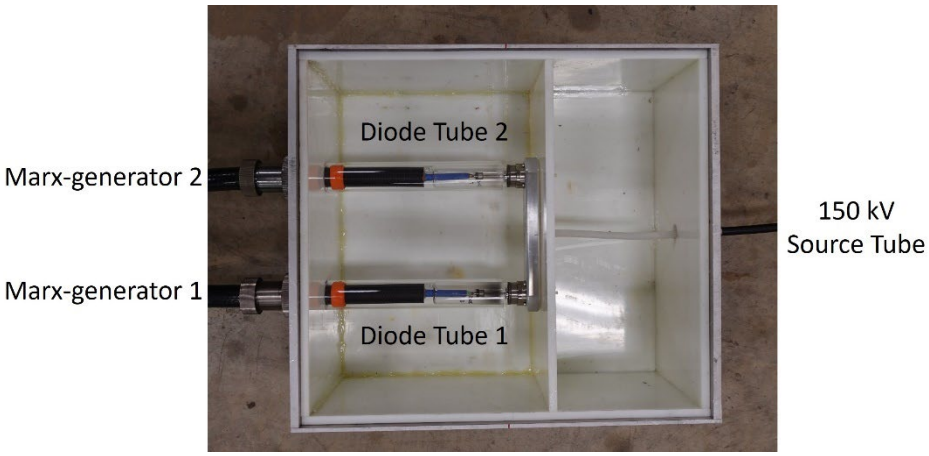

Fig. 5 Sequencer construction

The box is connected to two L3 300-kV pulsers via custom-ended Dielectric Sciences Inc. 2357 transmission lines.[8] The selected L3 300 kV systems use Marx generators to amplify charging potentials of approximately 30 kV to output potentials of approximately 300 kV and discharge currents near 5000 A. During the first attempt, we elected to use off-the-shelf L3 150-kV X-ray tubes (part no: 130-52900) as the field emission diodes. The tubes are readily available, robust to integration, and allowed observation of the diode's functionality via optical methods through the transparent glass body. The L3 150-kV systems, in which the 150 tubes are designed for use, use Marx generators to amplify charging potentials of approximately 29 kV to output potentials of approximately 150 kV and discharge currents near 2000 A. As supplied, both the 300-kV and 150-kV systems are balanced at 60 Ω to optimize the transmission of voltage to the load.[9–11] We intended to push power to a 120-Ω load, as we require a load consisting of two tubes organized in series. Also, because currents greater than 3000 A will be applied to 150 X-ray tubes that were designed to be used in a 2000-A system, we wanted to ensure that the hardware would be sufficiently robust to inhibit current flow. Because of these complications, and because we wanted to identify the electrical conduction path, we designed a series of experiments of increasing system complexity to observe current flow throughout isolated segments of the system.

The first experiments compared pulser functionality of a nominal L3 300 kV system and a system in which an L3 300-kV system powered two 150-kV tubes in series by monitoring the output of the pulser's capacitive voltage divider (CVD). This signal is designed to mimic the high-voltage field created near the top of the Marx generator stack. Figure 6 shows a schematic of the 300-kV driven experimental setup. Figure 7 shows two CVD traces from the nominal L3 300-kV system, and a CVD trace from the custom system shown in Fig. 6. The nominal system has good reproducibility, with a trace that also compares well to that published by the manufacturer. The bulk of X-ray generation occurs from the positive-going portion of the discharge within the first approximately 100 ns. Within this time, the CVD output of the custom X-ray sequencer system is very similar to the stock performance. Differences do arise in the continuing pulse, which can likely be attributed to impedance differences of the system. The inlay within Fig. 7 shows the CVD traces over approximately 10-µs duration. This overlay shows that the X-ray sequencer dissipates the field more quickly and does not indicate any late-time features that would suggest potential damage of the system.

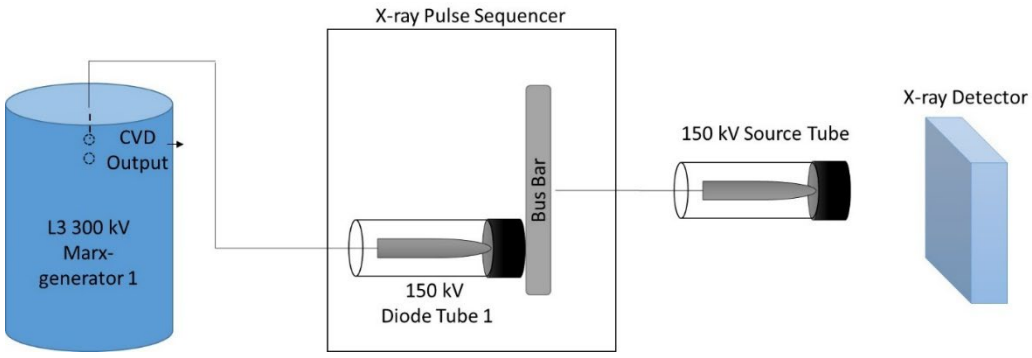

Fig. 6 Schematic of first experiments in which an L3 300 kV Marx generator was used to drive two 150-kV-rated tubes in series

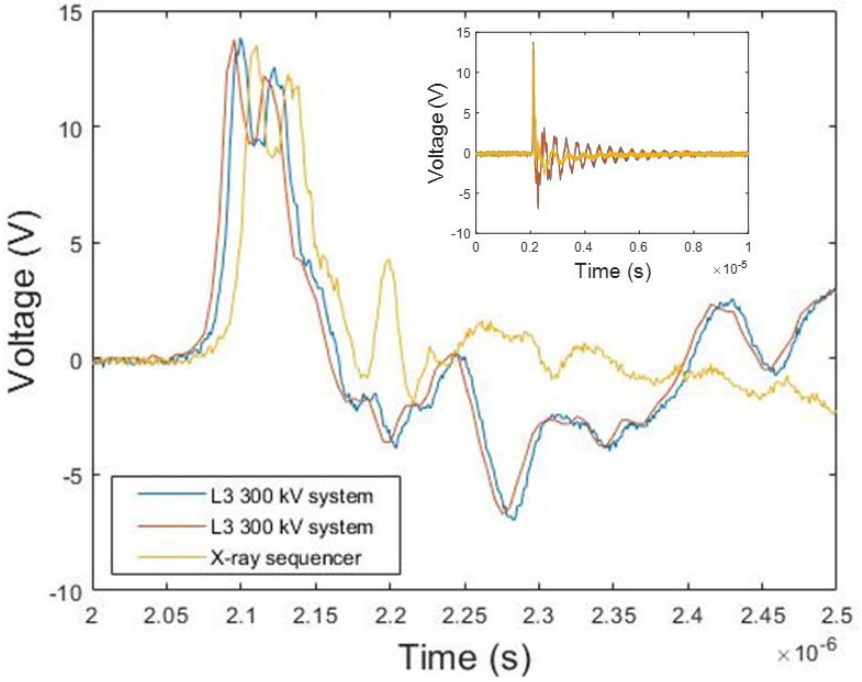

Fig. 7 CVD output for nominal L3 300-kV system and an L3 300-kV system connected to two 150-kV tubes in series as depicted in Fig. 6. The inlay shows the outputs plotted over a 10-μs duration.

When comparing the X-ray generation of the custom X-ray sequencer system to a nominal L3 150-kV system, the overall flux was found to decrease by approximately 70%. This comparison only considered X-ray generation from the source tube and isolated X-rays generated from the diode tube inside the X-ray pulse sequencer. The drop in dose is hypothesized to derive from current leakage to ground via air-jump and surface arcing within the sequencer. This hypothesis was derived considering optical observation (presented later in this section), showing plasma creation in unwanted regions of the custom system. This suggests more insulation is needed in the design to accurately determine output dosage. Although the dose was reduced, image resolution from both systems was comparable.

The second set of experiments investigated the ability of a field emission diode to resist high-voltage current flow. In this set of experiments, a second diode tube was added to the X-ray pulse sequencer box, with its anode connected to ground through a precision gap. Additionally, an inductive Pearson model 110 current monitor[12] was used to assess the current. Figure 8 shows a schematic of the experimental configuration used. The gap was left in open air and a Shimadzu HPV-X2 camera[13] was used to determine if conduction occurred via arching across the leads. By stepping through decreasing gap spacing, the Pashen curve[6,7] can be used to approximate the threshold standoff potential for reverse current. Table 1 lists some

experiments conducted and relevant parameters. These tests were conducted on January 26, 2022, at the US Army Combat Capabilities Development Command (DEVCOM) Army Research Laboratory's Aberdeen Proving Ground Experimental Facility 14 and used the larger, second version of the sequencer box shown in Fig. 5. For experiments 30–36, additional acrylic tubing offset by orange-colored electrical tape was added on the input legs for additional insulation (depicted in Fig. 5), which was not included during experiments 20–30.

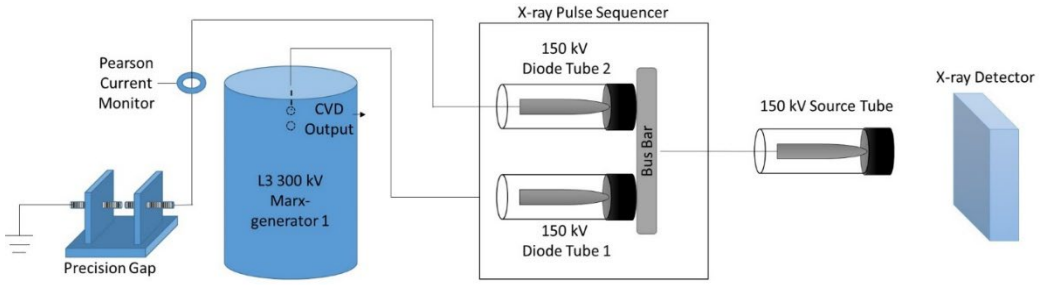

Fig. 8 Schematic of the second set of experiments to explore the ability of a field emission diode to resist high-voltage current flow

Table 1 Specifics of experiments used to determine current flow in the X-ray adder system

Experiment number	Main pulser discharge time (μs)	Secondary pulser discharge time (μs)	Line 2 termination	Target	Radiograph	Shimadzu field of view (fps)	Gap response
20	20	. . .	Open	Static	Good	Tubes (5M, failed timing)	. . .
21	20	. . .	Open	Static	Good	Tubes (5M)	. . .
22	20	. . .	3-mm gap to ground	Static	Good	Tubes (5M)	. . .
23	20	. . .	Grounded	Static	Good	Tubes (5M)	. . .
24	20	. . .	Open	Static	Good	Tubes (10M)	. . .
25	20	. . .	10-mm gap to ground	Static	Good	Gap (10M)	No
26	20	. . .	6.3-mm gap to ground	Static	Good	Gap (10M)	No
27	20	. . .	3-mm gap to ground	Static	Good	Gap (10M)	No
28	20	. . .	1.2-mm gap to ground	Static	Good	Gap (10M)	Arc
29	20	. . .	2-mm gap to ground	Static	Good	Gap (10M)	No
30	20	. . .	Secondary pulser (not charged)	Static	Good +	Tubes (5M)	. . .

Table 1 Specifics of experiments used to determine current flow in the X-ray adder system (continued)

Experiment number	Main pulser discharge time (µs)	Secondary pulser discharge time (µs)	Line 2 termination	Target	Radiograph	Shimadzu field of view (fps)	Gap response
31	20	. . .	Secondary pulser (not charged)	Static	Good +	Tubes (1M)	. . .
32	20 (misfire)	200 (misfire)	Secondary pulser	Static	Good +	Tubes (1M)	. . .
33	20	200	Secondary pulser	Static	Good +	Tubes (1M)	. . .
34	20	200	Secondary pulser	Dynamic	Single	Tubes (1M)	. . .
35	20	1000	Secondary pulser	Dynamic	Double	Tubes (250k)	. . .
36	20	50	Secondary pulser	Dynamic	Single	Tubes (5M)	. . .

Notes: M = million; k = thousand

The precision gap tests concluded that for a gap of 2 mm, which equates to approximately 7.5-kV threshold, conduction did not occur. When reduced to 1.2 mm, which equates to approximately 5-kV threshold, conduction does occur. All tests, regardless of conduction, produced similar quality radiographs. Figure 9 confirms conduction by showing frames of the precision gap from both experiments at the time of Marx generator discharge and 100 ns after discharge. Confirmation of timing synchronization is performed using star-anomalies detection in the optical images. The star-anomalies arise from X-ray interactions with the Shimadzu HPV-X2 sensor. In these experiments, the camera used a frame rate of 10,000,000 frames per second (fps). Pulse discharge and X-ray generation occurred in frames 48 and 49 of experiments 28 and 29, respectively.

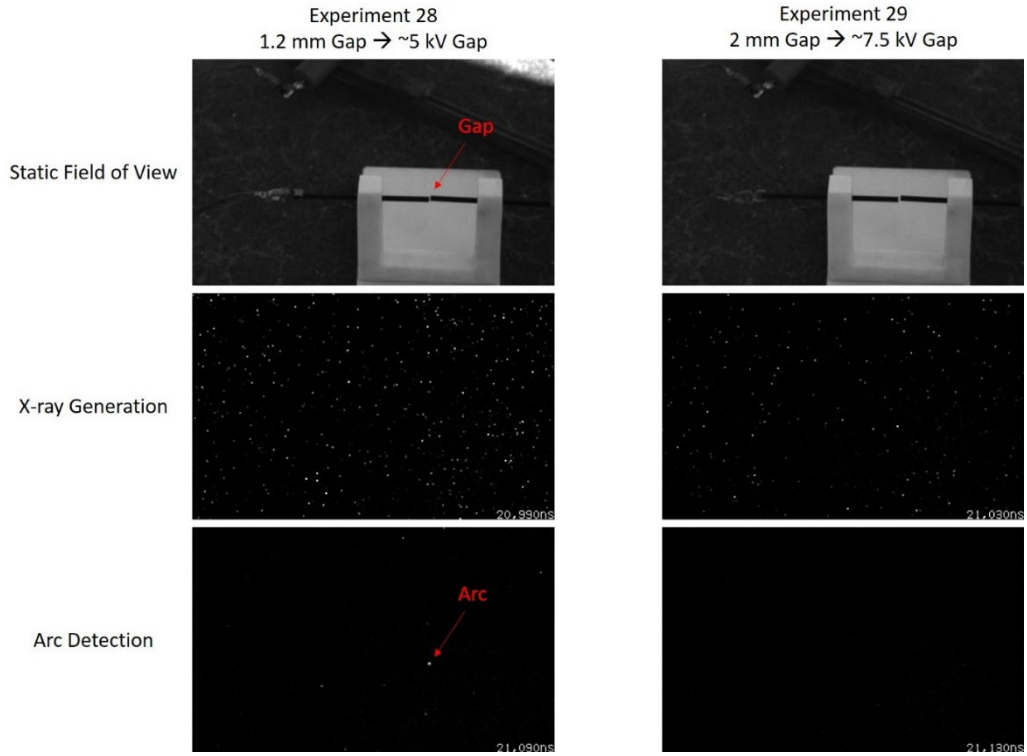

Fig. 9 Precision gap during experiments that assessed reverse current conduction through a field emission diode

The model 110 Pearson monitor, which outputs 0.1 volts per amp, was connected to an Agilent DSO6104A oscilloscope using a 20×, 50-Ω attenuator and a ground loop interrupter. This results in approximately a 40× reduction in the recorded signal voltage. Figure 10 shows the Pearson signals from multiple gap experiments. As can be seen from experiments in which no conduction was detected via optical means, the Pearson monitor suffered from significant background noise during Marx generator discharge. This is hypothesized to result from coupling of the emitted electromagnetic pulse and/or potentially varying ground levels associated with pulse discharge. Without compensating for the background noise, the highest voltage detected during the 1.2-mm gap test in which conduction occurred was 0.84375 V. This corresponds to 337.5 A, suggesting that even when arcing is detected, the current operating through the field emission diodes in the reverse orientation is minimal. Further, the L3 300-kV system output is balanced to deliver 5000 A into a 60-Ω load. Because the X-ray sequencer approximately doubles the load impedance, we would expect to observe 2500–3300 A through the X-ray source tube when current flows as intended. This correlates with the observation that all experiments produced similar quality radiographs, as approximately 90% or more of the current was conducted along the intended path to the X-ray source tube.

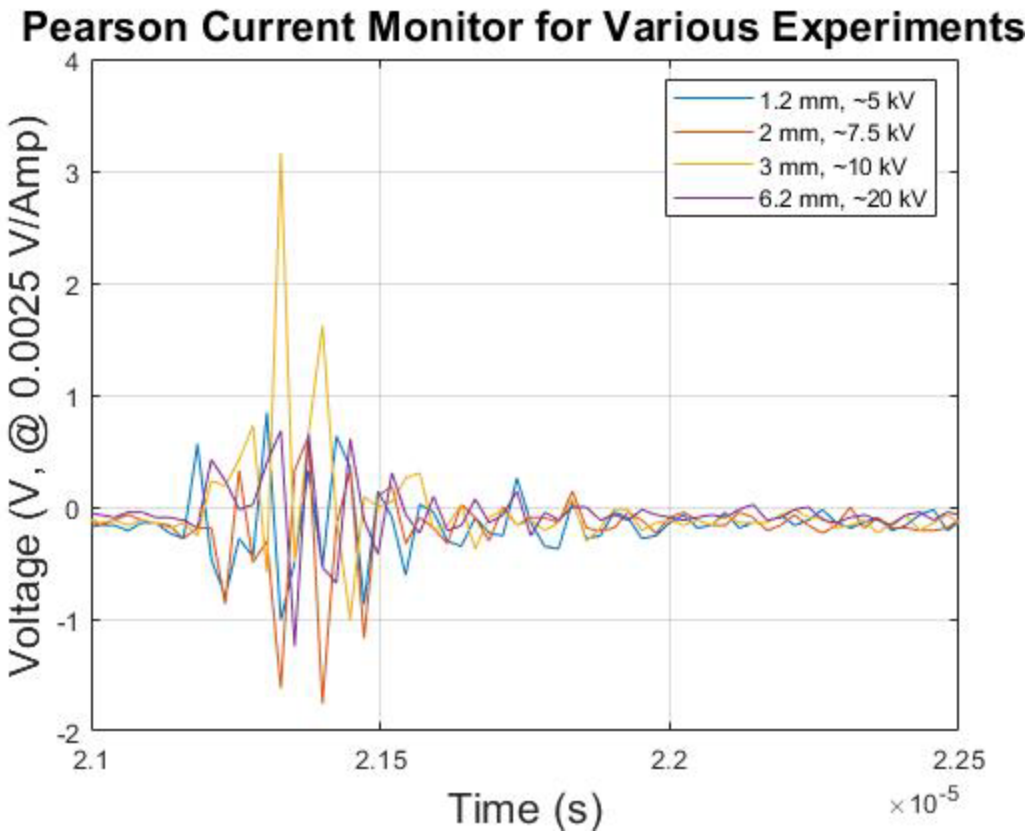

Fig. 10 Pearson current monitor signals from experiments in which conduction through the field emission diode did and did not occur

High-speed photography of the diode tubes within the X-ray sequencer also confirms the current paths. Figure 11 shows optical photographs of light generated during select experiments in which line 2 termination was varied. The images were collected at 5,000,000 fps. The left-most images were acquired close to discharge, as identified by star-anomalies throughout. The middle and right images are the following sequential frames (discharge +200 ns and discharge +400 ns). The light of interest is that near the diode gap, assumed to be generated from a plasma that is created upon conduction within the tube.

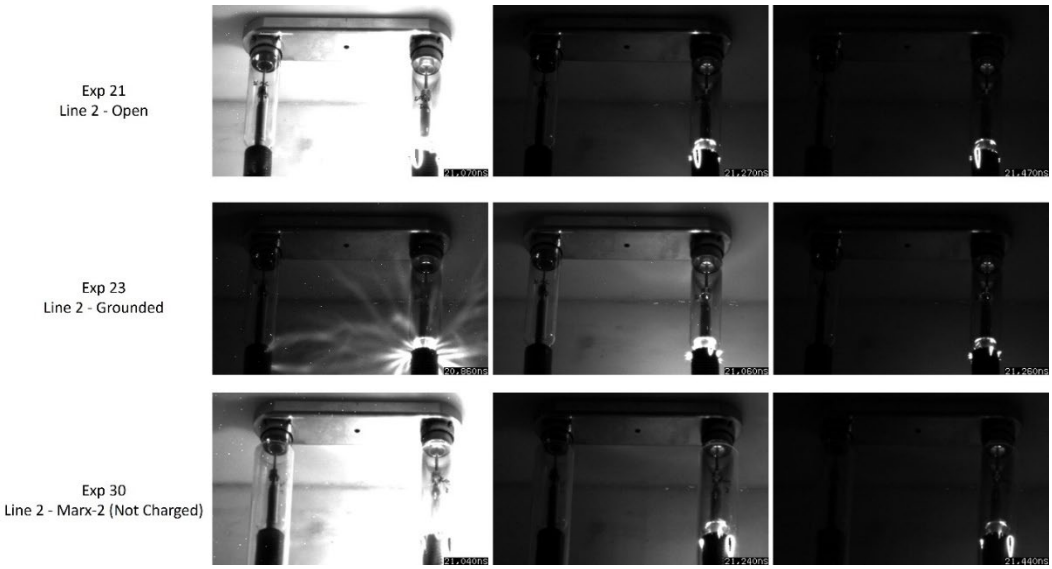

Fig. 11 Optical photographs of the X-ray sequencer during pulse discharge. In these experiments, only the line 1 systems were pulsed. Within the images diode 1 is on the right and diode 2 is on the left.

There is a stark difference between the initial image captured for experiment 23 in which line 2 was grounded compared to the other two experiments in which line 2 was floating. We are unsure if this is a realistic difference, or if it was a manifestation of timing related to the electrical pulse width, camera gate length, and interframe spacing. The relatively high intensity of the second image in experiment 23, compared to experiments 21 and 30, suggests that discharge in the previous frame was captured near its gate end, therefore revealing the discharge structure seen. It also could be that the grounded cable/tube joint allowed an alternate conduction pathway to dissipate some of the current. Regardless, all series demonstrate that only the diode 1 tubes generate light at the diode-gap, suggesting minimal or no conduction occurs along the diode 2 path. If conduction did occur, the late-time images (pictured on the right) indicate that light emissions from an arc or plasma generation are undetectable by 400 ns after the initial discharge. The isolation of the desired path is further supported by the similar quality radiographs that were produced during the experiments regardless of line 2 termination.

Figure 12 shows a similar series of photographs acquired during experiment 34 with image times at t = 21, 200, 201, and 202 μs. In this experiment, line 1 was connected to Marx generator 1 and line 2 was connected to Marx generator 2. Marx generator 1 was discharged at t = 20 μs, and Marx generator 2 was discharged at t = 200 μs. The radiographs imaged a drill spinning a bent metal hex-wrench at approximately 765 rpm. The discharge of Marx generator 1 indicated light generation occurred within diode 1 only. The upper right panel of Fig. 12 (t = 200 μs) shows that light emissions continue within diode 1 up to the time at which Marx generator 2

discharged. Upon discharge, diode 2 flashes brightly, and diode 1 moderately increases its light intensity. The light generation at diode 1 suggests reverse conduction across the diode. Although the relative intensity of the plasma in diode 2 was greater than that of diode 1 during the Marx generator 2 discharge, no conclusions can be made as to the magnitude of the currents. We hypothesize that the allowance of reverse current was likely caused by the remaining plasma shorting the diode, precluding the intended operation where a lack of field concentration would inhibit field emission of electrons propagating from the tungsten cathode to the pointed tips on the surrounding anode. Although no noticeable effects were imposed on the Marx generator 1, this is not ideal.

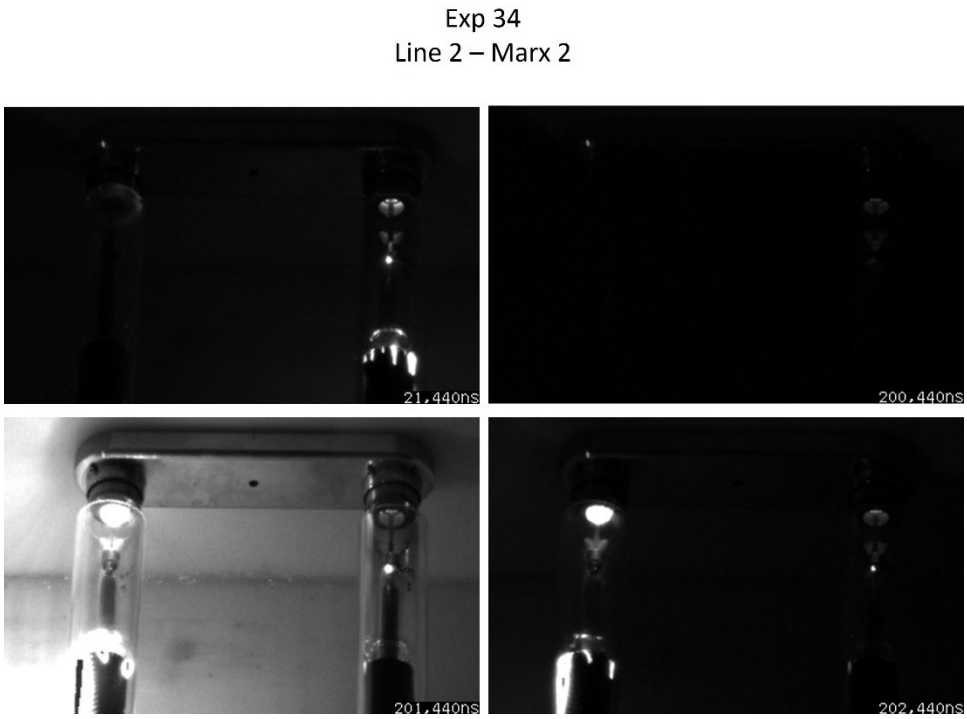

Fig. 12 Optical photographs of the X-ray sequencer during experiment 34. In this experiment, line 1 system was pulsed near 20 µs, and the line 2 system was pulsed near 200 µs. Within the images, diode 1 is on the right and diode 2 is on the left.

Figure 13 shows a photograph of the drill with hex-wrench target, and the radiograph acquired during experiment 34. The 180-µs difference in discharge time should have produced an overlaid image in which the hex-wrench rotated approximately 0.83°, counterclockwise. Inspection of the image shows a very faint second image, appearing as a shadow or blurring of the hex-wrench. The poor quality radiographic second image is likely linked to the alternate current path, referenced in the preceding paragraph, reducing the current supplied to create the second X-ray pulse. Although the X-ray source tube is similar to the diode tubes, persistence of plasma within this tube's gap should not preclude X-ray production,

as the rod-pinch mechanisms should continue to produce bremsstrahlung radiation.[14–20] It is known, however, that controlling the initial plasma and the diode geometry can optimize bremsstrahlung radiation output.[21,22]

Fig. 13 Radiographic target (drill with a bent hex-wrench) and radiographic image from experiment 34 in which two electrical pulses were supplied to the X-ray sequencer 180 μs apart.

Figures 14 and 15 show optical and radiographic results from experiment 35, which is a repeat of experiment 34, with an increased separation of the Marx generator discharge to 980 μs. Figure 14 shows complete dissipation of the light generated within diode 1 before Marx generator 2 is discharged. It also shows that diode 1 does not relight after discharge of Marx generator 2. Although the light generation has not been rigorously correlated with conductive properties of the diode, the results support the hypothesis that the light is connected to plasma existence, and its dissipation is needed to functionalize the field emission effect diodes. Figure 15 corroborates this, showing functionality of the X-ray pulse sequencer in which two images of the drill show the hex-wrench rotated by 4.5° counterclockwise.

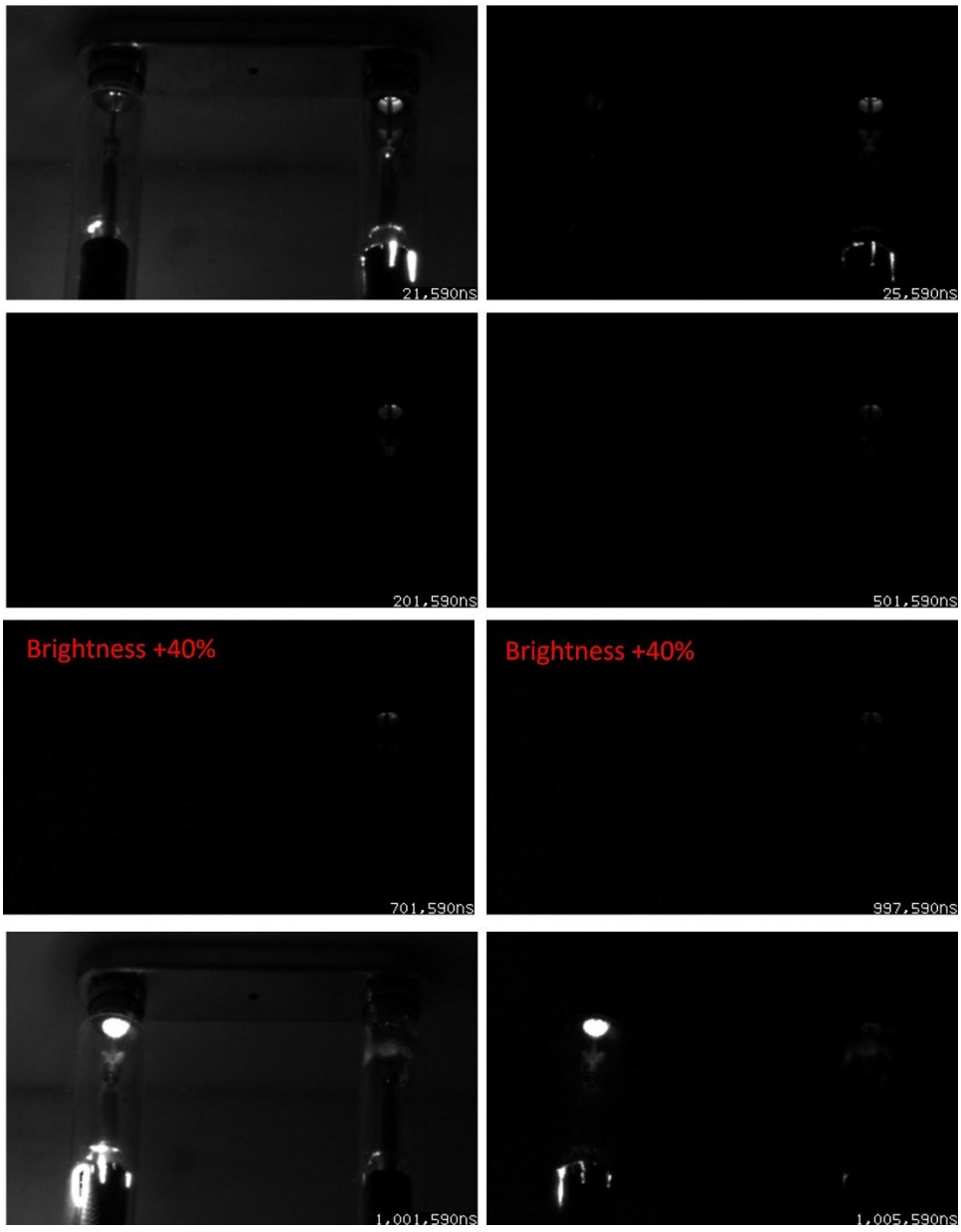

Fig. 14 High-speed photography frames

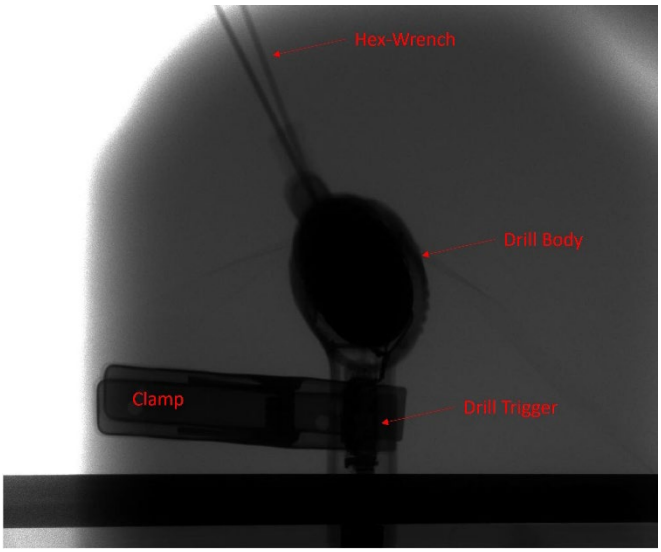

Fig. 15 X-ray radiograph

2.2 Plasma Characterization

As alluded to in the Section 2.1, Field Emission Effect Diode Method, the generation of plasma at the gap within the field emission effect diode is strongly linked to the ability to control functionality for multi-pulse X-ray generation using the sequencer. Plasma is generated when high-speed electrons impact the tungsten anode.[16,17] The electron impact causes local heating, which desorbs trapped gases at the anode surface. These gases are subsequently ionized, creating a plasma. Because plasmas are inherently conductive,[23,24] the existence of plasma bridging the diode gap has potential to short its functionality. For this reason, the ability to control the plasma generation and lifespan are desired. The ability to manipulate the plasma, however, is strongly correlated with its makeup (i.e., its species, temperature, and vector velocity). Although the initial plasma interactions are defined by Coulomb interactions used to generate the X-rays, thermal properties will contribute as the plasma persists.

Although we have not yet determined the precise threshold at which plasma influences the diode functionality (i.e., allowing conduction), we can apply the assumption that minimization, and preferably elimination, of the plasma will improve functionality. We also assume that, because the initial plasma generation mechanism does not change, light detected from diode-generated plasma is directly correlated to the quantity of plasma persisting.[25,26] Therefore, the ability to influence the light generated within the diode gap suggests our ability to influence its electrical functionality.

To study plasma within field emission diodes, custom hardware was created to allow for optical observation. The first piece was like that shown in Fig. 5, but was more compact, using spacings of approximately 5.6 cm needed to insulate a 150-kV load. Figure 16 shows the hardware configured such that one input leg was removed and the output shorted, to essentially create an open-viewing, single tube system.

Fig. 16 Hardware to allow observation of plasma within off-the-shelf field emission X-ray tubes. Pulser (aside to the left).

Although plasma generated inside an L3 150-kV vacuum tube using an L3 150-kV source may have some differences to that generated using two L3 150-kV tubes in series and an L3 300-kV source, we assume sufficient similarity to demonstrate general phenomenology. This series of experiments assess the baseline plasma and if it can be altered using a magnetic field. The species of the plasma is assumed to consist primarily of protons (938.28 MeV/c2) from the relatively low atomic mass trapped surface gases,[16,17] with extremes including possibilities of tungsten ions (171846 MeV/c2) and free electrons (0.511 MeV/c2). The charged ions and electrons within the plasma will interact with the magnetic field via the Lorentz force:

$$F = q * (v \times B) \tag{1}$$

where q is the charge, v is the particle velocity, and B is the magnetic field vector. The initial 150-kV accelerating potential can be used to approximate upper velocity threshold. This yields 5.36e6 m/s (1.79% speed of light) for the protons, 3.96e5 m/s (0.13% speed of light) for the tungsten ions and 1.9e8 m/s (63.4% speed of light) for electrons.

To assess if the persistent plasma has preferred directionality, we examined the plasma volume and lifespan using high-speed optical photography while applying magnetic fields across the diode. These experiments used permanent magnets to create the field. Permanent magnets have the potential to influence X-ray

generation[27–29]; however, they are much easier to integrate for probing experiments compared to pulsed electromagnetics, which could be switched on after X-ray generation. Table 2 summarizes relevant parameters from experiments executed on February 24, 2022.

Table 2 Parameters of experiments probing influence of magnetic fields on plasmas within glass-based X-ray tubes

Experiment number	Notes	Magnetic field inside cathode cup (mTesla, traverse)	Magnetic field inside cathode cup (mTesla, axial)	Magnetic field outside cathode cup (mTesla, traverse)	Magnetic field outside cathode cup (mTesla, axial)	Shimadzu frame rate (fps)
5	. . .	. . .	. . .	. . .	. . .	500,000
6	. . .	. . .	. . .	. . .	. . .	500,000
7	. . .	. . .	. . .	. . .	. . .	500,000
8	Apply transverse field	2	3	103	15	500,000
9	. . .	2	3	103	15	500,000
	Calibration	. . .	. . .	. . .	. . .	500,000
10	Applied axial field	2	3	14	103	500,000
11	. . .	2	3	14	103	500,000
12	Reversed axial field direction	2	3	16	105	500,000
13	. . .	2	3	16	105	500,000
14	. . .	2	3	16	105	500,000

One complication with this series of experiments was the ability to generate the magnetic field inside the metallic cathode structure of the glass-based X-ray tubes. Two magnetic configurations were explored. The first configuration established a transverse field, with the primary B vector oriented perpendicular to the anode axis. This field was generated by placing two 1-inch cube neodymium (NdFeB) magnets on either side of the X-ray tube with their north poles aligned similarly and perpendicular to the anode axis. The NdFeB magnets have a magnetic field of approximately 0.5 T near their polar surfaces. The second configuration established a field in which the primary B vector was oriented parallel to the anode axis. This field was generated by placing three 1-inch cubed NdFeB magnets around the X-ray tube with their north poles aligned parallel the anode axis. Figure 17 shows these configurations. Figure 18 shows a photograph of a cathode structure removed from a tube, with indication of where the anode interacts. A LakeShore 410 Gaussmeter (Hall probe) was used to map the fields within and external to the cup. The field inside the cathode was found to reduce 2 orders of magnitude compared to outside, because of the metallic cup's shielding influence (acting like a Faraday cage).

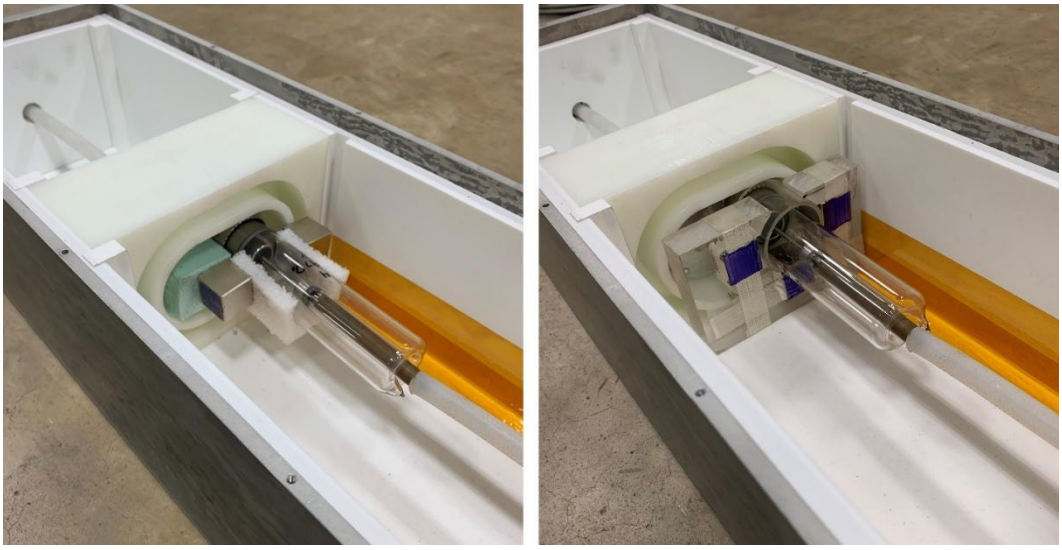

Fig. 17 Magnet configurations used to generate fields inside glass-based X-ray tubes. South poles of the magnet are colored blue to indicate magnetic field orientation.

Fig. 18 Cathode cup removed from an L3 150-kV X-ray tube. The geometry shields the ability to inject magnetic field into the region where the anode interacts with the cathode plane.

Figure 19 shows optical photographs of the diode after the pulse discharge for the multiple nonmagnetic and magnetic configurations. The dashed green box outlines the region of interest in which the plasma is of concern. Figure 20 shows the integrated light intensity within the region of interest as a function of time. These experiments were unsuccessful at clearly defining any magnetic influence on the plasma structure properties, as the shot-to-shot variability overpowered any response due to the dependent variable.

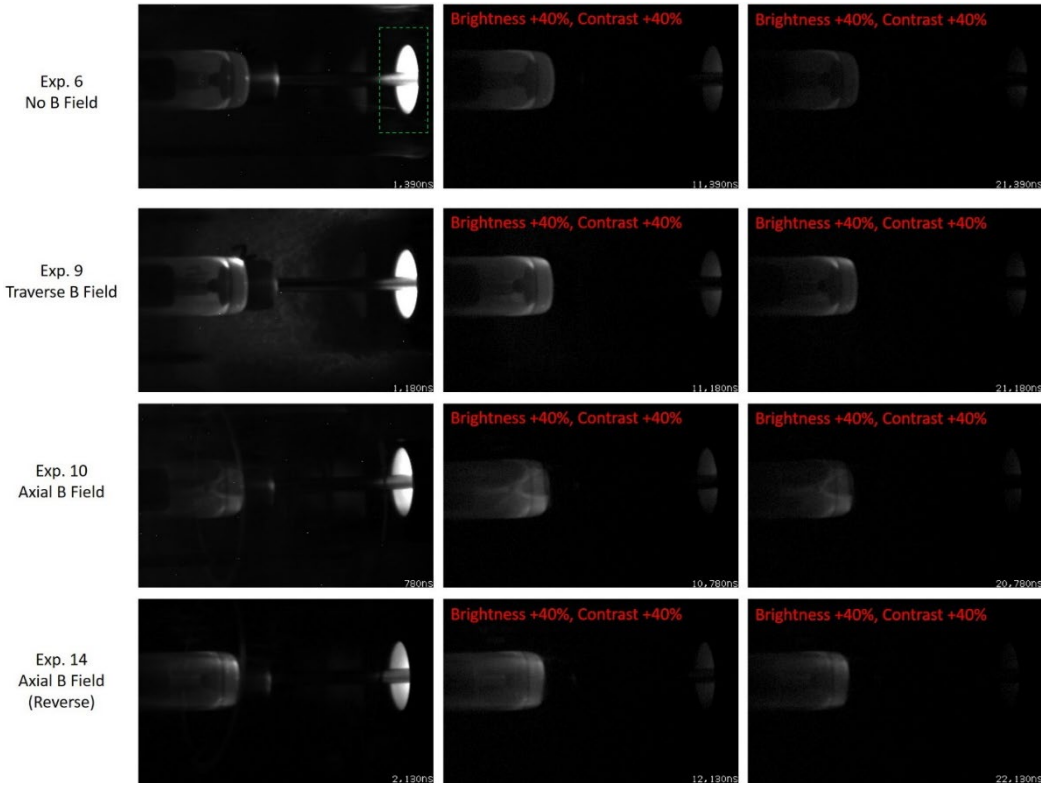

Fig. 19 Optical photography of the plasma generated inside X-ray vacuum tubes with and without application of magnetic fields

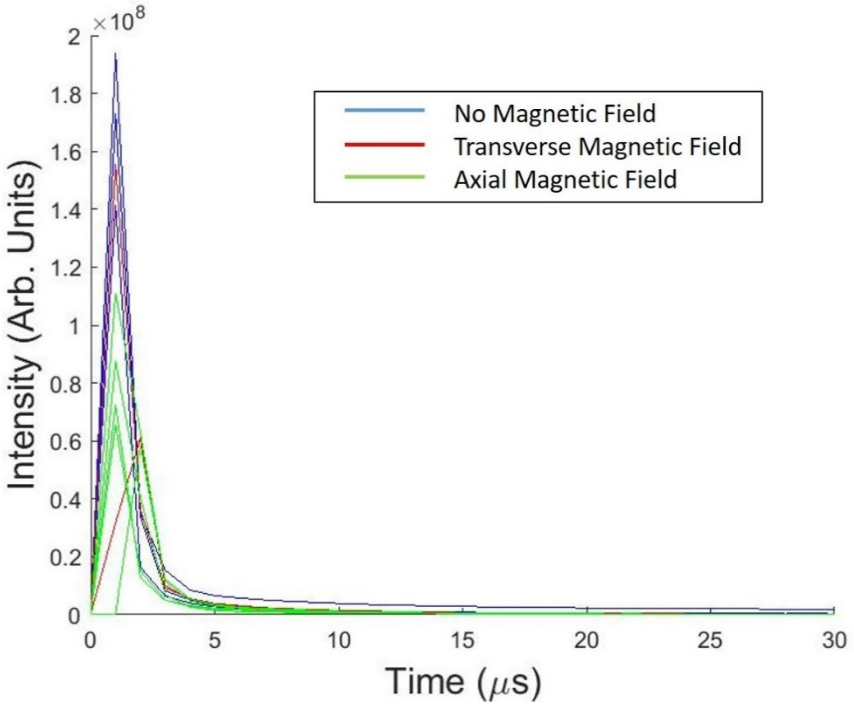

Fig. 20 Light intensity within the region of interest of glass-based X-ray tube diodes throughout and after electrical pulse discharge

To increase the magnitude of the field injected into the diode region, experiments were conducted using a Scandiflash XT 300L tube.[30] The tube was modified to include a transparent polycarbonate window to allow observation of the plasma. The system used an adapter and cable extension to allow the tube to be connected to an L3 150-kV pulser. The head was evacuated to a pressure of approximately 3.6×10^{-6} mTorr. Figure 21 shows the modified Scandiflash tube and adapting components. The Scandiflash XT 300L tube was fit with a Scandiflash D10 cathode that has a 9.9-mm diameter, and a Scandiflash F1 anode that has a 1.6-mm diameter in the plane of the cathode. When approximated as a transmission line with a dielectric constant of 1 (vacuum), this geometry results in 109.2 Ω of impedance. This will result in approximately 50% losses in both the transmitted voltage and power delivered to the diode in comparison to the 60-Ω balanced, glass-based vacuum tubes that transmit 100% of the voltage and approximately 45% of the power.[10,11]

Fig. 21 Modifications of a Scandiflash XT 300L tube to include a transparent front cover and adapters to fit to an L3 150-kV pulser

Table 3 summarizes the experiments conducted March 3–9, 2022, exploring the influence of magnetic fields on the plasma generated at the Scandiflash diode. Without any external influences, the heat and ablation that occurs during each pulse causes decay of the relatively small anode at a noticeable rate. Figure 22 plots the X-ray dose for experiments in which no magnetic field was applied. A linear fit to

the data shows a 0.17% decrease in dose for each experiment, with significant noise observed. Figure 23 shows an optical characterization of this phenomenon using photographs of the light in the diode region of interest approximately 10 μs after pulse discharge. Figure 23 also shows the integrated light within the diode region of interest as a function of time. The optical response, assumed to correlate with the plasma cloud, appears to be more sensitive to the anode degradation process than the radiographic dose analysis. Because of this decay, assessments comparing magnetic field influences will be compared to nonmagnetic experiments conducted just prior to, and just following, the magnetic experiments.

Table 3 Summary of experiments conducted using the Scandiflash diode with and without application of magnetic fields

Experiment number	Notes	Magnetic field in front of cathode (mTesla, traverse/ axial)	Magnetic field at cathode (mTesla, traverse/ axial)	Magnetic field behind cathode (mTesla, traverse/axial)	Magnetic field far behind cathode (mTesla, traverse/axial)
17	Baseline	. . .	. . .	. . .	. . .
18	Baseline	. . .	. . .	. . .	. . .
19	Baseline	. . .	. . .	. . .	. . .
20	Add X-ray detector	. . .	. . .	. . .	. . .
21	Magnet (north up)	30/90	70/125	90/140	180/70
22	Magnet (north up)	30/90	70/125	90/140	180/70
23	Magnet (north up), add X-ray resolution target	30/90	70/125	90/140	180/70
24	Magnet (north up)	30/90	70/125	90/140	180/70
25	No magnet	. . .	. . .	. . .	. . .
26	No magnet	. . .	. . .	. . .	. . .
27	No magnet	. . .	. . .	. . .	. . .
28	No magnet, add offset X-ray resolution target	. . .	. . .	. . .	. . .
29	No magnet	. . .	. . .	. . .	. . .
30	No magnet	. . .	. . .	. . .	. . .
31	Magnet (north up)	30/90	70/125	90/140	180/70
32	Magnet (north up)	30/90	70/125	90/140	180/70
33	Magnet (north up)	30/90	70/125	90/140	180/70
34	No magnet	. . .	. . .	. . .	. . .
35	No magnet	. . .	. . .	. . .	. . .
36	No magnet	. . .	. . .	. . .	. . .
37	Magnet (north backward)	150/50	140/20	210/50	180/140
38	Magnet (north backward)	150/50	140/20	210/50	180/140

Table 3 Summary of experiments conducted using the Scandiflash diode with and without application of magnetic fields (continued)

Experiment number	Notes	Magnetic field in front of cathode (mTesla, traverse/ axial)	Magnetic field at cathode (mTesla, traverse/ axial)	Magnetic field behind cathode (mTesla, traverse/axial)	Magnetic field far behind cathode (mTesla, traverse/axial)
39	Magnet (north backward)	150/50	140/20	210/50	180/140
40	No magnet	. . .	. . .	. . .	. . .
41	No magnet	. . .	. . .	. . .	. . .
42	No magnet	. . .	. . .	. . .	. . .
43	Magnet (north forward)	135/35	150/20	220/80	150/140
44	Magnet (north forward)	135/35	150/20	220/80	150/140
45	Magnet (north forward)	135/35	150/20	220/80	150/140
46	Magnet (north forward)	135/35	150/20	220/80	150/140
47	Magnet (north right)	5/0.1	10/2	10/5	12/15
48	Magnet (north right)	5/0.1	10/2	10/5	12/15
49	Magnet (north right)	5/0.1	10/2	10/5	12/15
50	No magnet	. . .	. . .	. . .	. . .
51	No magnet	. . .	. . .	. . .	. . .
52	No magnet	. . .	. . .	. . .	. . .

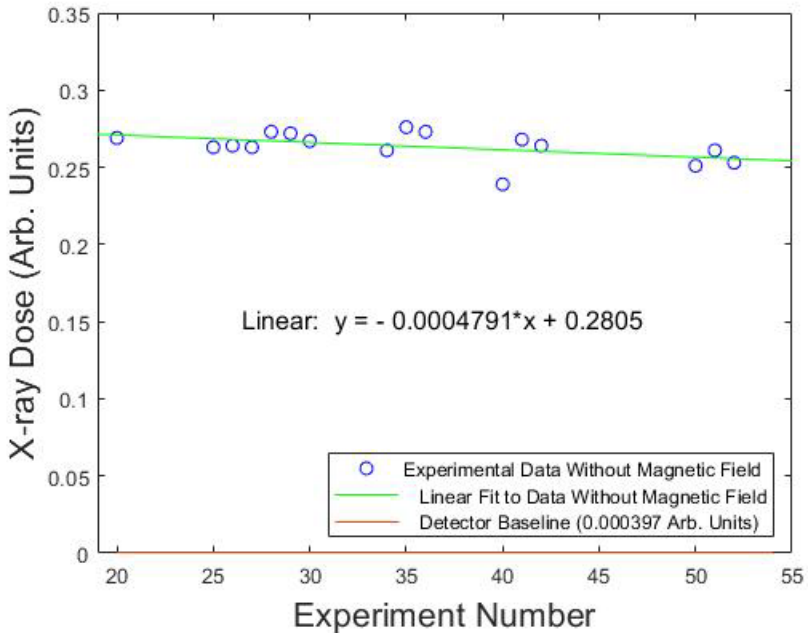

Fig. 22 X-ray dose measured for multiple experiments

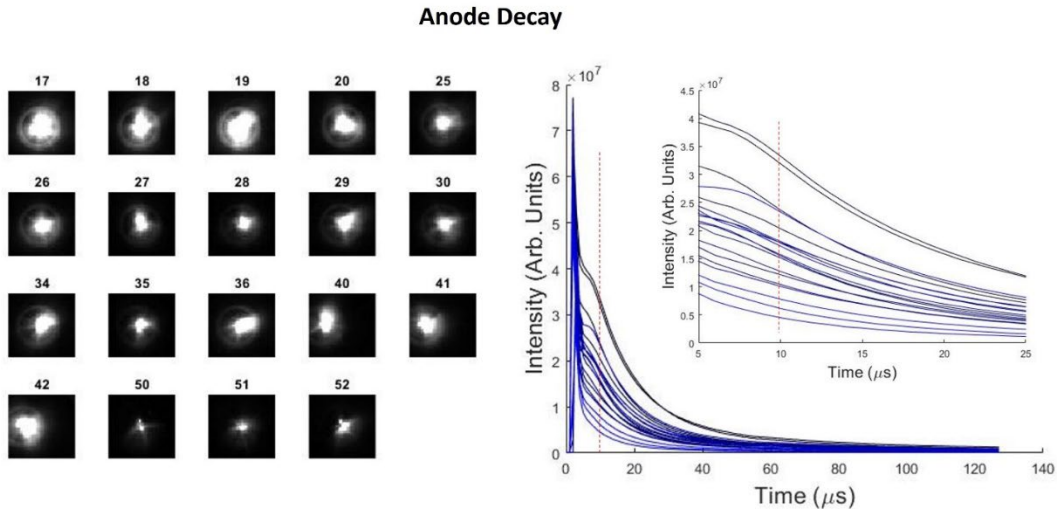

Fig. 23 Optical characterization of anode decay within the Scandiflash XT 300L diode. The photographs on the left were acquired 10 μs after pulse discharge. This time is indicated by a dashed red line overlaid on the decay curves (right). The decay curves (and zoomed inlay) were colored using a linearly graded scheme in order from earliest (black, experiment 17) to last acquired (blue, experiment 52).

Figures 24–28 show the setup geometries and influence of applied magnetic fields on the plasma and X-ray generation of the diode. Although the geometry of the magnet and setup are quite simplistic, the field injected into the diode region is complicated by the metal components of the Scandiflash XT head. Figure 29 shows a mapping of the magnetic field vectors for the magnetic north pole pointed up and pointed forward along three slices extracted from within the diode region. One slice was located toward the X-ray output side (forward, positive Z), one located at the cathode plane (Z = 0), and one located behind the cathode plane (negative Z). In these quiver plots, the arrow lengths are scaled to the magnitude of the field vector. For these two cases, the field injected near the cathode is approximately orthogonal, with the north pole up orientation of the magnet creating a field that is mostly parallel with the anode and the north pole forward orientation of the magnet creating a field that is mostly perpendicular to the anode. The field magnitudes near the anode surface at the cathode plane for all magnetic field orientations are quantified in Table 3. These values are intended to relate general trends for the multiple orientations, while the quiver plots identify the overall field geometry.

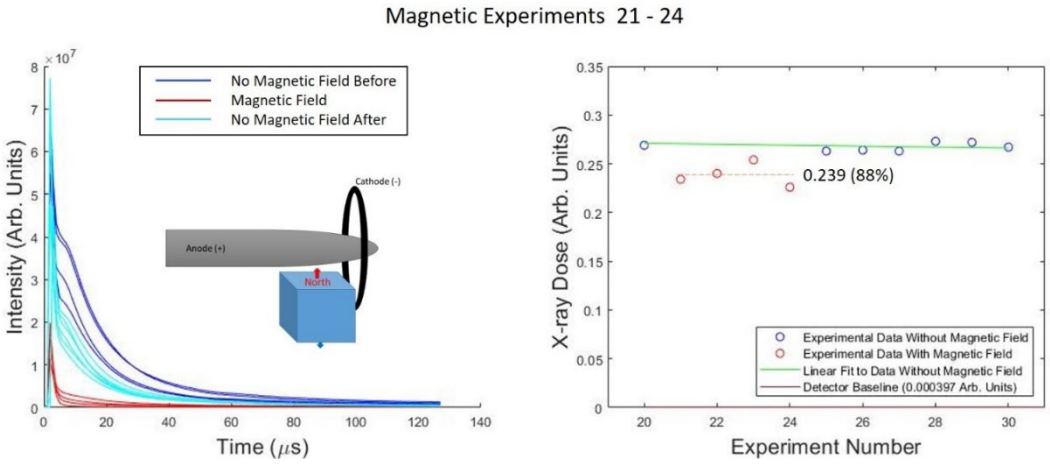

Fig. 24 Influence of north-pole-upward orientation of the magnetic field on the plasma and X-ray generation

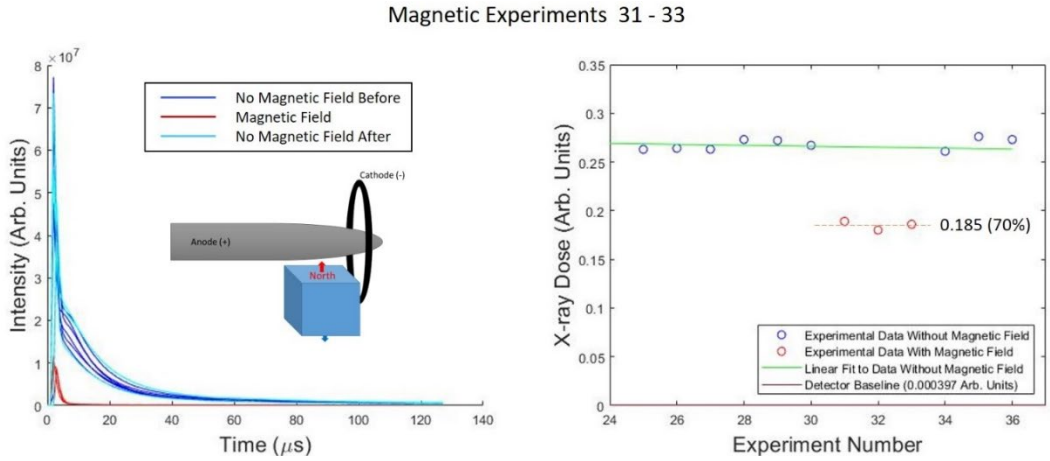

Fig. 25 Influence of north-pole-upward orientation of the magnetic field on the plasma and X-ray generation (repeat)

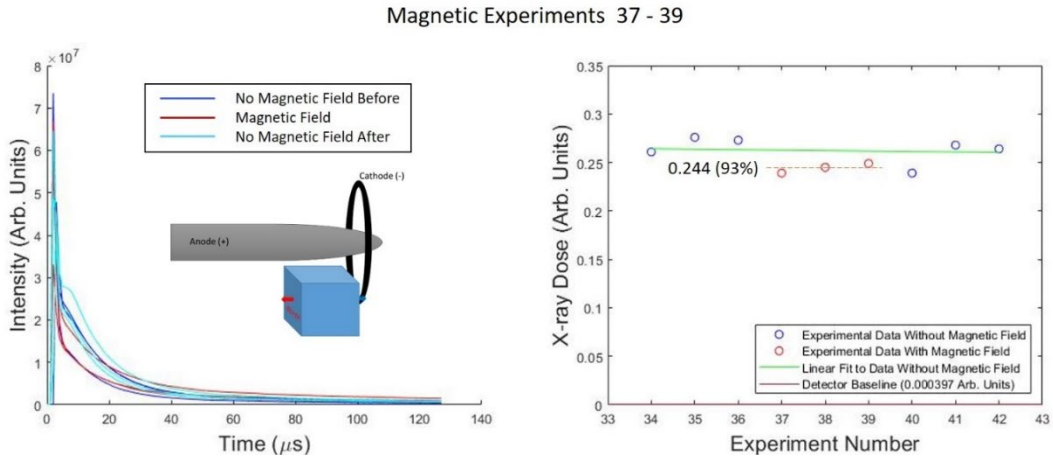

Fig. 26 Influence of north-pole-backward orientation of the magnetic field on the plasma and X-ray generation

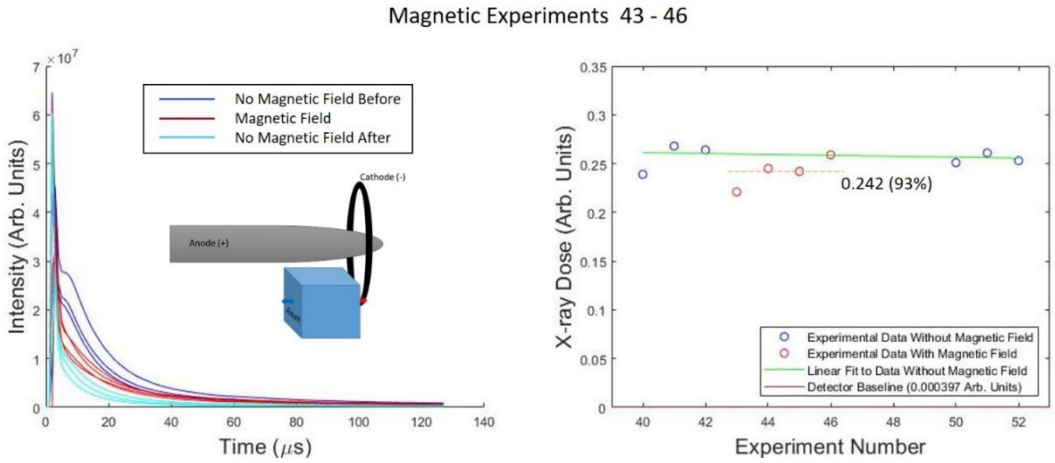

Fig. 27 Influence of north-pole-forward orientation of the magnetic field on the plasma and X-ray generation

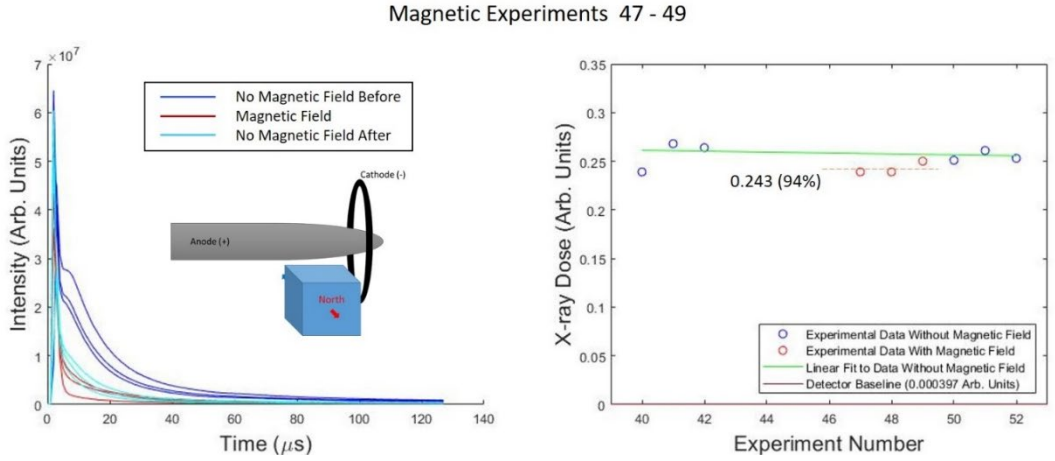

Fig. 28 Influence of north-pole-sideway orientation of the magnetic field on the plasma and X-ray generation

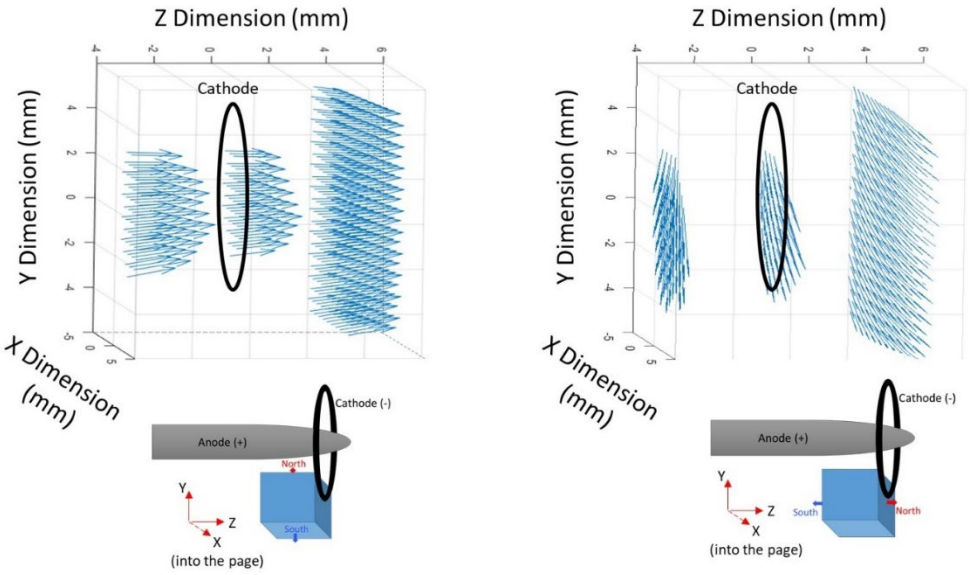

Fig. 29 Magnetic field vector mapping for the north-pole-up (left) and north-pole-forward (right) orientations of a permanent magnet inserted in a Scandiflash XT300 tube. The cathode plane lies parallel to the X-Y plane centered at X = 0, Y = 0, and Z = 0.

Generally, the presence of a magnetic field imposed small variations on the X-ray production. This is important because any influence on the X-ray production could imply influence on the electron current at the diode gap. The magnetic field influences X-ray generation through Lorentz force interactions with the high-speed electrons prior to tungsten anode impact. In alternate work, application of a magnetic field was intentionally performed to focus and enhance electron beams for X-ray generation.[27–29] In our geometry, the electric field is sufficient to supply a corrective force to trajectory deflections imposed by the applied magnetic field, ultimately resulting in most electrons impacting the anode. Empirically, the measured X-ray dose was found to decrease, in one case producing as low as 70% of the nominal dose, with an average dose reduced to 88%.

Although introduction of a magnetic field would likely only be applied to the diodes within the sequencer and not the X-ray source tube, it was observed that the image resolution was not found to be negatively influenced. Here implications as to the electron impact spot size as a result of the applied magnetic field can be deduced. The image resolution was tested using a Leeds Test Object Type 23 CN 60129 with lines per millimeter (LP/mm) ranging from 0.5 to 5.0 across the test object as shown in Fig. 30. The figure shows results from experiment 24 (magnet north pole up) with the test object located at approximately 15 mm from the surface of the detector. The lineouts of the radiograph at 1.0 and 2.0 LP/mm yield a scale of 0.137 and 0.138 mm/pixel, respectively, which is consistent with a detector pixel size of 0.139 mm and a source-to-detector distance of 1.53 m. The test object was then

placed 0.92 m from the source. Resolution was compared at 0.7 and 1.0 LP/mm at this standoff location for experiments 28–52. Generally, there was no observable loss of resolution. In fact, a direct comparison between experiments 47–49 (inserted magnet north to the right) and 50–52 (no magnet) showed an increase in resolution for radiographs 47–49, indicated by greater contrast across the lines of the test object (i.e., less blurring). This is shown in Fig. 31, which indicates 32.5% and 27.0% larger average oscillation amplitude for 0.7 and 1.0 LP/mm, respectively, across the test object lines. Figure 32a shows that the shot-to-shot variation for a given experimental setup is extremely low, producing nominally identical responses. However, each applied field did not account for better resolution. Figure 32b shows that experiments 31 and 32, which had applied fields (north up), produced resolution nominally identical to the no field cases. Also shown are two no-field cases (30 and 50) separated by many X-ray pulses, which had resolution remaining essentially unchanged.

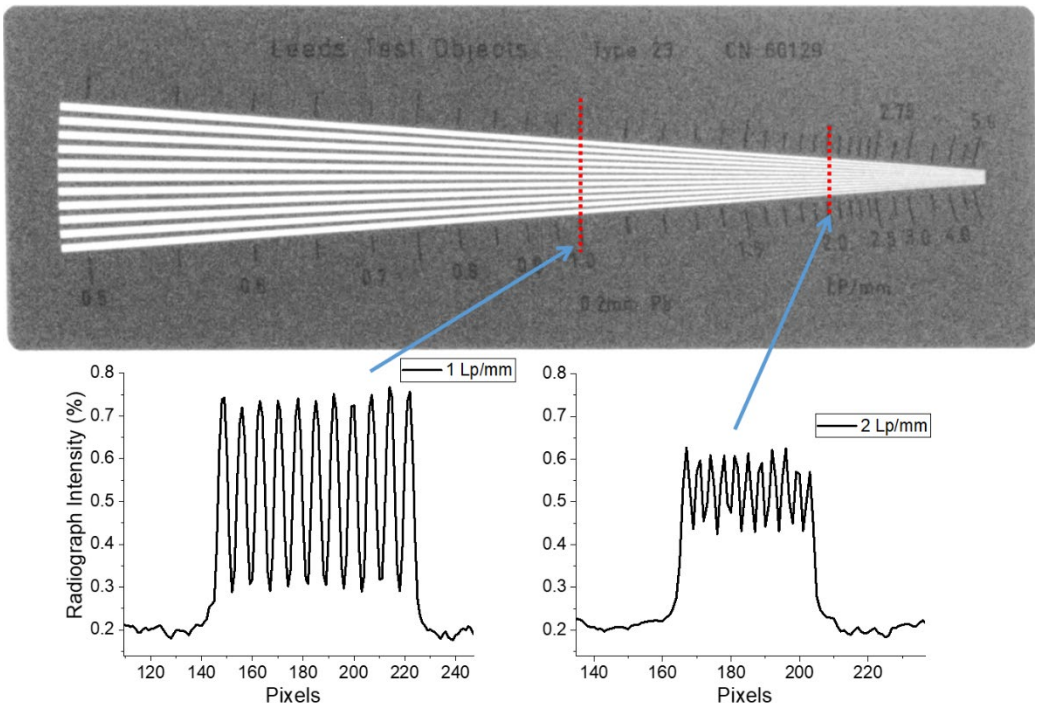

Fig. 30 Leeds test object and lineouts from shot 24 (magnet inserted, north-pole-up) at 1 and 2 LP/mm. The contrast and brightness on the image were modified for greater visibility of the test object.

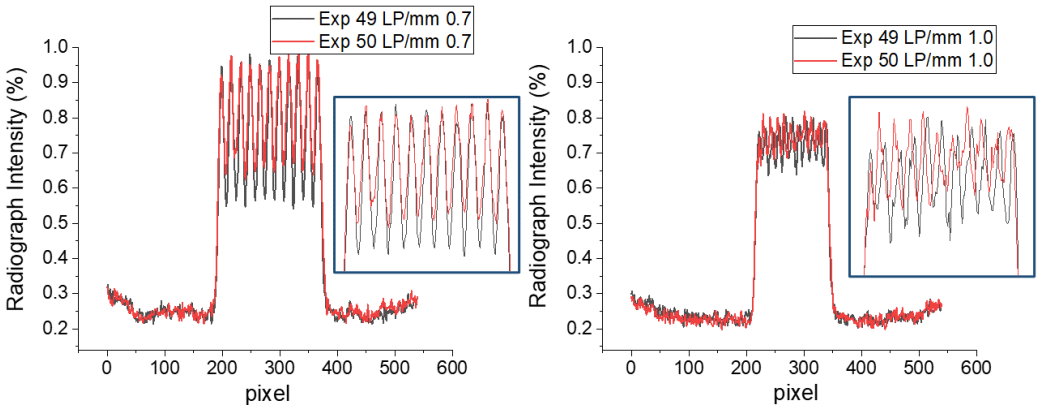

Fig. 31 Lineouts from Leeds test object when placed at 0.92 m from the X-ray source. A comparison between experiments 49 (applied magnetic field, north-pole-to-the-right) and 50 (no field).

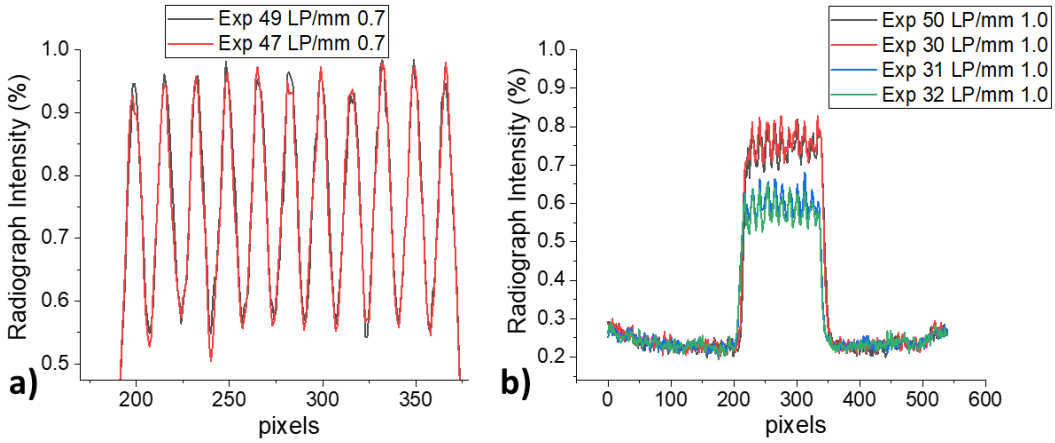

Fig. 32 Lineouts a) from experiments 47 and 49 (identical applied magnetic fields) and b) from experiments 30 and 50 (no field), and 31 and 32 (applied field)

To perform a direct comparison for the experiments where the total X-ray dose was reduced, the line scans across the test object were scaled to a relative intensity from 0 to 1. This is shown in Fig. 33 where experiments 28 (no magnet) and 33 (north-up magnet inserted) are compared. Figure 34 shows the average amplitude of the intensity oscillations across the lines for experiments 28–52. The solid gray line at 0.4075 represents the average of all amplitudes from the no-magnet experimental conditions. The shaded area represents 1 standard deviation from the no-magnet data (0.0176). This closer inspection reveals that in the magnet case with north pointing backward, a drop of about 9% in resolution occurred (just within 2 standard deviations of the inherent variation in the no-magnet data). The orientation of the applied magnetic field does appear to affect the resolution, but generally increases resolution. It is postulated that the field in some configurations localizes the electron impact on the anode reducing the source spot size.

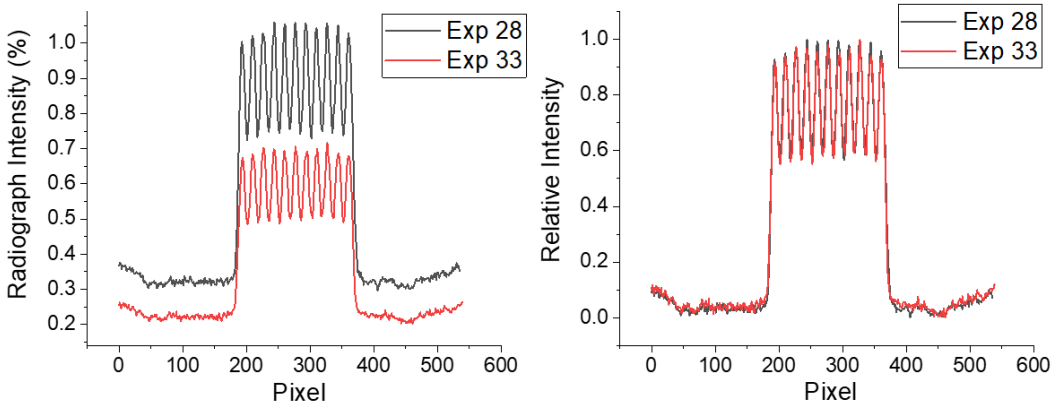

Fig. 33 Lineouts from experiments 28 (no magnet) and 33 (magnet, north-up), which caused a reduced dose. The lineouts in the right plot are scaled to the X-ray dose, the ones on the left are not.

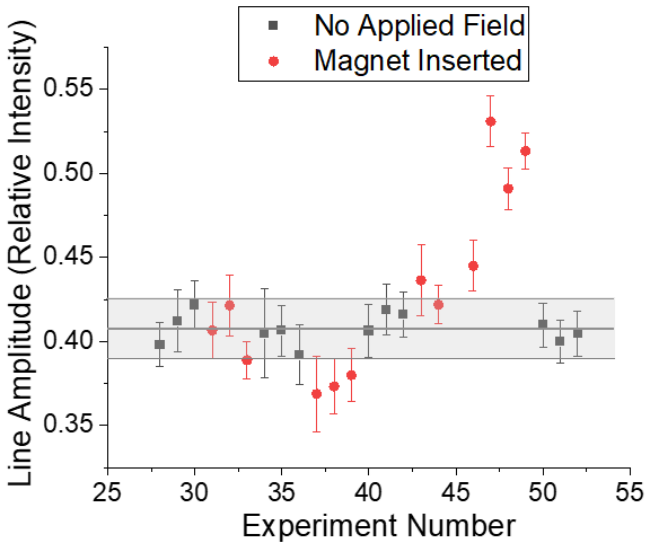

Fig. 34 Average oscillation amplitude from the lineouts across the test object for each experiment with the offset test object

The optical characterization showed a more dramatic response to application of external magnetic fields than X-ray production. This was found to depend on the field orientation, suggesting the plasma within the diode does have a preferred directionality. Light generation from within plasma occurs through electron-ion collision processes. These include ionization, excitation, de-excitation, and electron-ion recombination.[25,26] All these processes will be influenced by the presence of a magnetic field, either directly through magnetic modification of atomic states or indirectly through processes such as the influence of scattering cross section through the alteration of particle trajectory. Using the assumption that our plasma consists primarily of protons, the later likely dominates. Our observations of light generally show a quick onset to maximum light, followed by

decay. When the magnet was oriented with the north pole pointed upward, the most favorable results were achieved, shortening the time of light decay. In this orientation, the magnetic field near the plane of the cathode had a large axial component (see Fig. 29). Based on the schematics of how electrons and ions primarily interact within rod-pinch diodes,[17] this field orientation was anticipated to have a strong coupling through the Lorentz force during early times near X-ray generation. However, it appears that the persistent plasma in the diode gap ($t \geq 1$ μs) also has a preferred velocity orientation. In alternate B field orientations that favored axial field orientations near the cathode plane, little or no influence was observed in the light response. These results support conclusions that the persistent plasma has a directional preference and that using a magnetic field to assist in the dissipation of the plasma could be optimized. Modeling the plasma as it shifts from Coulombic-force-structured to thermally equilibrated may help with understanding its orientation evolution.

3. Future Designs and Discussion

The current X-ray sequencer has demonstrated success at combining multiple pulses. However, a few modifications may improve the design. These modifications could work to potentially increase the X-ray dose through enhanced currents while sequencing or reduce the pulse separation timing. The first suggestion is to increase the insulation factor to isolate potential current leakage to ground. This can easily be done by increasing the component standoff or by using dielectric material to insulate and isolate desired pathways. Because potential leakage pathways may be unknown, one of the most obvious techniques that could be applied is to fill the sequencer box with mineral oil or some other dielectric fluid. This would maximize the insulation factor and eliminate potential surface arcing pathways.

To reduce the time between flashing, we suggest modifying functionality to prohibit plasma from shorting the diode gaps. We successfully demonstrated that application of a permanent magnetic field can influence the plasma due to its persistent structure, however, multiple time-dependent and/or directional fields could be applied. Electromagnets could be used to apply pulsed magnetic fields generated from external-circuit coils, eliminating any complications of influencing the initial electrons that generate the X-rays. Similar efforts have been successfully integrated for enhanced electron beam production.[27–29] Integration schemes can easily isolate such components from the high-voltage potentials of the X-ray generation system. Magnetic field strength could also be controlled by the design of the pulsed power applied. Regardless of using permanent magnets or

electromagnets, field directionality is a relatively simple matter so long as sufficient space is available to insert coils or permanent magnets.

Another possibility is the use of electric fields to control the plasma through the Coulombic interactions rather than magnetic fields via the Lorentz force. This, however, would require large potentials as the thermal energy of plasmas is large. If it could be implemented, using an electric field may provide better control of the direction, as it would not rely on the plasma constituents' velocities.

Any attempt to inject electromagnetic fields in general may also benefit from using "nonmagnetic" materials in the diode construction. For example, one may want to change the cathode material from the ferromagnetic iron-based material. Materials such as aluminum may provide benefit. Elimination of materials that influence the magnetic field drastically or metals that would neutralize electric fields may be useful.

Because the diodes within the X-ray sequencer are not desired to produce X-rays, material choice decisions can also be made to optimize the field emission effect for the anode materials. Materials such as steel or graphite could be used. Likewise, geometry considerations could also be optimized. For example, one could design the anode to have a hemispherical end to minimize the field effect emissions when a reverse bias is applied. One could also design the diode to have a more optimal geometry to be influenced by electromagnetic fields for plasma sweeping. Ideas such as implementing a singular pointed cathode instead of a disk-shaped cathode may be useful.

It may also be possible to use a physical barrier to preclude the plasma from shorting the diodes within the sequencer unit. The plasma is generated from the anode surface heating associated with electron impingement. If an electron-permeable membrane was placed between the anode and cathode, it may be possible to allow the high-potential electrons to penetrate the membrane for X-ray generation but resist the passage of protons and ions that cause diode shorting. Although the high-temperature plasma will be abrasive, materials such as thin layers of Kapton tape could provide such functionality. Multiple geometries are possible, ranging from adding a coating directly to the tungsten anode surface to adding a barrier of material suspended in the gap between the anode and cathode.

4. Conclusion

We have demonstrated functionality of a field emission effect high-voltage diode-based multi-pulse X-ray sequencer that produces multiple X-ray pulses out of a single X-ray diode. This functionality was demonstrated for inter-pulse delays of

approximately 1 ms. The inter-pulse timing was correlated with plasma generation that shorts the diode gap.

It was also demonstrated that permanent magnets can be used inside a X-ray diode to influence the plasma lifespan. This was correlated via observation of the plasma light emission. It was shown that the plasma lifespan can be shortened with minimal influence on X-ray generation. Alternate methods to improve the output flux of the sequencer and the inter-pulse timing of the X-rays were provided.

5. References

1. Wood RW. A new form of cathode discharge and the production of X-rays, together with some notes on diffraction. Preliminary communication. Physical Review (Series I). 1897;5(1):1.

2. Dyke WP, Dolan WW. Field emission, in advances in electronics and electron physics. Marton L, editor. 1956, Academic Press. p. 89–185.

3. Fowler RH, Nordheim L. Electron emission in intense electric fields. Proceedings of the Royal Society of London. Series A, Containing Papers of a Mathematical and Physical Character. 1928;119(781):173–181.

4. Pulserad. Flash X-ray systems. Specialized Imaging (Formerly L3). [accessed 2022 Apr 13]. https://www.specialised-imaging.com/products/intensifiers/flash-x-ray.

5. Drury D, Childers K, Pomeroy S, Lau D, Link N, Laurence P, Creely B, Kolkana R, Sousa D. L3 flash Xray seminar, L-3 Pulse Sciences, San Leandro, California.

6. Paschen F. Ueber die zum funkenübergang in luft: wasserstoff und kohlensäure bei verschiedenen drucken erforderliche potentialdifferenz. 1889:JA Barth.

7. Husain E, Nema RS Analysis of paschen curves for air, N2 and SF6 using the Townsend breakdown equation. IEEE Transactions on Electrical Insulation. 1982;EI-17(4):350–353.

8. Dielectric Sciences, Inc. 2357 transmission lines. [accessed 2022 Apr 13]. https://www.dielectricsciences.com/.

9. Espenschied L, Herman AA, inventors. Concentric conducting system. United States patent US 1,835,031. 1931.

10. Lampen S. 50 ohms the forgotten impedance. 2012 Aug 27 [accessed 2022 Apr 13]. https://www.belden.com/blogs/broadcast/50-ohms-the-forgotten-impedance/.

11. Belzer EC. Some contributions of the Bell Laboratories in the development of communications. School Science and Mathematics. 1950;50(8):652–654.

12. Pearson Electronics. Model 110 current monitor. [accessed 2022 Apr 13]. https://www.pearsonelectronics.com/.

13. Shimadzu. HPV-X2 camera. [accessed 2022 Apr 13]. https://www.shimadzu.com/an/products/materials-testing/high-speed-video-camera/hyper-vision-hpv-x2/index.html.

14. Blaugrund A, Cooperstein G. Intense focusing of relativistic electrons by collapsing hollow beams. Physical Review Letters. 1975;34(8):461.

15. Blaugrund A, Cooperstein G, Goldstein SA. Processes governing pinch formation in diodes. In: 1975 International Topical Conference on Electron Beam Research & Technology. IEEE; 1975.

16. Blaugrund A, Cooperstein G, Goldstein SA. Relativistic electron beam pinch formation processes in low impedance diodes. The physics of fluids. 1977;20(7):1185–1194.

17. Cooperstein G, Boller JR, Commisso RJ, Hinshelwood DD, Mosher D, Ottinger PF, Schumer JW, Stephanakis SJ, Swanekamp SB, Weber BV, et al. Theoretical modeling and experimental characterization of a rod-pinch diode. Physics of Plasmas. 2001;8(10):4618–4636.

18. Mahaffey RA, Golden J, Goldstein SA, Cooperstein G. Intense electron-beam pinch formation and propagation in rod pinch diodes. Applied Physics Letters. 1978;33(9):795–797.

19. Young FC, Commisso RJ, Allen RJ, Mosher D, Swanekamp SB, Cooperstein G, Bayol F, Charre P, Garrigues A, Gonzales C, et al. Rod-pinch diode operation at 2 to 4 MV for high resolution pulsed radiography. Physics of Plasmas. 2002;9(11):4815–4818.

20. Swanekamp SB, Commisso RJ, Cooperstein G, Ottinger PF, Schumer JW. Particle-in-cell simulations of high-power cylindrical electron beam diodes. Physics of Plasmas. 2000;7(12):5214–5222.

21. Weber B, Cooperstein D, Hinshelwood D, Mosher D, Schumer JW, Stephanakis SJ, Strasburg SB, Swanekamp SB, Yount FC. The plasma-filled rod-pinch diode: a new technique to concentrate MeV electron beams to ultra-high power and energy densities. In: AIP Conference Proceedings. American Institute of Physics; 2002.

22. Weber BV, Allen RJ, Commisso RJ, Cooperstein G, Hinshelwood DD, Mosher D, Murphy DP, Ottinger PF, Phipps DG, Schumer JW, et al. Radiographic properties of plasma-filled rod-pinch diodes. IEEE Transactions on Plasma Science. 2008;36(2):443–456.

23. Bittencourt JA. Fundamentals of plasma physics. Springer Science & Business Media; 2004.

24. Gurnett DA, Bhattacharjee A. Introduction to plasma physics: with space and laboratory applications. Cambridge University Press; 2005.

25. Hahn Y. Electron-ion recombination processes-an overview. Reports on Progress in Physics. 1997;60(7):691.

26. Ali S. Electron-ion recombination data for plasma applications: results from electron beam ion trap and ion storage ring. Department of Physics, Stockholm University; 2012.

27. Friedman M, Ury M. Production and focusing of a high power relativistic annular electron beam. Review of Scientific Instruments. 1970;41(9):1334–1335.

28. Maenchen JE, Gustwiller J, Johnson DL, Molina I, Olson C, Rosenthal S, Rovang D, Oliver B, Welch D, Bailey V, et al. Inductive voltage adder driven X-ray sources for hydrodynamic radiography. In 12th IEEE International Pulsed Power Conference. Institute of Electrical and Electronic Engineers; 1999.

29. Mazarakis MG, Maenchen JE, Rovang DC, Menge PR, Lash JS, Smith DL, Johnson DL, Halbleib JA, Cordova SR, Mikkelson K, et al. Inductive voltage adder (IVA) for submillimeter radius electron beam. in 11th IEEE International Pulsed Power Conference. Institute of Electrical and Electronic Engineers; 1997.

30. Scandiflash AB. XT 300L tube. [accessed 2022 Apr 13]. https://scandiflash.com/.

List of Symbols, Abbreviations, and Acronyms

ARL	Army Research Laboratory
CVD	capacitive voltage divider
DEVCOM	US Army Combat Capabilities Development Command
fps	frames per second
LP/mm	lines per millimeter
NdFeB	neodymium

1 (PDF)	DEFENSE TECHNICAL INFORMATION CTR DTIC OCA
1 (PDF)	DEVCOM ARL FCDD RLD DCI TECH LIB
7 (PDF)	DEVCOM ARL FCDD RLW TA W UHLIG B WILMER P BERNING FCDD RLW TD M ZELLNER J SHOWALTER B HUNTZINGER FCDD RLW TE N STURGILL